then U_i(exp.) < U_i(calc.). This case indicates that the experiments show that cavitation inception is at a lower speed than that predicted by the theoretical calculations and thus the prediction is non-conservative. On the other hand, when

$$\sigma_i(\text{exp}) < \sigma_i(\text{calc.})$$

or U_i(exp) > U_i(calc.), the predicted values for cavitation inception are conservative.

Figure 16, which is a comparison of calculated and experimentally observed cavitation index for the 3-bladed propeller 4132 (EAR = 0.3), shows conservative predictions when J = 0.7 or design J, whereas the predictions are non-conservative, somewhat at J = 0.6 and especially so at J = 0.5, except near the hub and near the tip. In Figures 17 and 18, for the 3-bladed propellers 4118 (EAR = 0.6) and 4133 (EAR = 1.2), respectively, all predictions are on the conservative side except those for J = 0.5.

Judging from this set of calculations, the predicted values of cavitation inception are on the conservative side compared with experimental observations as long as $\Delta J = J_d - J_{od} < 0.3$. Nevertheless, the discrepancies which exist between predicted values of the index of cavitation inception and the experimental observations require investigation.

These observed discrepancies must not be solely attributed to the lack of accuracy of the linearized theory when modified by the Van Dyke correction. It is well known that visual determination of inception of cavitation is dependent upon the subjective evaluation of the observer and is highly dependent on the surface finish and accuracy of the model in the immediate vicinity of the leading edge of the blades. The variant patterns of the viscous flow at appreciable angles of attack can involve laminar separation with vortical flow standing off the blade surface giving extremely low pressures in the core of the vortex (as cited frequently by Eisenberg, for example) and, hence, inception at σ values larger than the minimum pressure coefficient provided by inviscid theory on the surface of the blade. Also, from the definitive measurements of Huang and Hannan[19], it can be conjectured that large pressure fluctuations can occur on the blade surface at the reattachment zone abaft laminar separation. In addition, it is never certain that observed inception is attributed to truly vaporous cavitation or to the expansion of undissolved air.

The fact that the experimental σ-values are generally higher than the calculated $|C_{p_m}|$ at the maximum excursion in J (i.e., J = 0.5, ΔJ = 0.33) suggests that the real fluid effects alluded to above may be responsible. However, at the larger J = 0.7 (smaller ΔJ = 0.13), the disagreement is in the opposite direction except for the first propeller, EAR = 0.30, where the agreement is fine. Here the fluid speeds are of the order of twice as great as at J = 0.5 and the pressure peaks on the blades at reduced angle of attack, while lower in magnitude, are indeed sharper, i.e., the chordwise width of the pressure spike is reduced. One may speculate that the passage time of nuclei through the region of low pressure is considerably less at J = 0.7 than at J = 0.5 (higher speed, shorter extent) and that cavitation does not ensue until the σ values are dropped below the $|C_{p_m}|$.

The validity of the theoretical curves should be checked by employing a rational method for finding the effective angle of attack, the effective camber and the effective thickness of the two-dimensional section (to be substituted for each bladesection) for which exact steady-state pressure distributions have been computed. This is not a simple process as was discovered when attempting to use the families of curves provided by Brockett[20] and a rule for finding the effective angle of attack attributed to W. Morgan. The effective angle of attack was found to be too imprecise; a very small error produces a larger error in the C_{p_m} value.

Clearly, further studies of the pressure distribution at the leading edge of propellers are necessary. The results obtained thus far should be regarded as quite reasonable. Further work may require a precise mechanization of the effective two-dimensional solutions using certain inputs from the three-dimensional propeller flow field, and local sectional loadings.

CONCLUSION

In this study, a theoretical approach is evolved and a computational procedure adaptable to a high-speed digital computer (CDC 6600 and 7600) is developed for evaluation of the linearized pressure distribution on each side of a marine propeller blade, with the objective to obtain sufficient and reliable information for cavitation and blade stress analyses.

The essential information for the blade stress analysis is the antisymmetric part of the blade pressure distribution, attributed to the nonuniform inflow (wake), blade camber, incident flow angle and nonplanar thickness of the blade, all of which are associated with the lifting action of the blade and contribute to the hydrodynamic forces and moments and blade bending moments. The symmetric part of the blade pressure distribution, attributed to the planar thickness and associated with the non-lifting properties of the blade, contributes to the pressure distribution on each side of the blade, which is essential for the prediction of cavitation inception.

In addition to the blade pressure distributions at each frequency, the program furnishes the propeller-generated steady-state and time-dependent hydrodynamic forces and moments and the blade bending moment about the face-pitch line at the midpoint of any of the radial strips into which the span is divided. The program also provides the instantaneous blade pressure due to loading alone and the instantaneous pressures on suction and pressure sides, as well as the instantaneous blade bending moments, as the propeller swings around its shaft. The thrust and torque due to friction is estimated by using an approximate frictional drag coefficient; in the event of any improvement of the estimated frictional coefficient, this portion of the program can be easily modified.

In applying the mode approach to the solution of the surface integral equation, the analysis and the program are divided into two main parts, one dealing with the steady-state flow case ($q = 0$) and the other with the unsteady flow condition. The steady-state case is subdivided into design and off-design conditions. The selection of the proper chordwise modes in the steady-state flow condition at design advance ratio J is dictated by the shape of the loading distribution in two-dimensional flow on a foil with the same camber distribution. At off-design J in the steady-

state condition, there is an angle of attack due to the difference ΔJ (between design and off-design advance ratio) and the additional loading due to this angle of attack is represented by the cotangent term of the Birnbaum modes. In the unsteady flow condition, the complete Birnbaum modes are used.

The linearized unsteady lifting-surface theory requires the leading-edge singularity arising from the cotangent term of the Birnbaum modes. The "square-root" singularity is integrable, but its presence in the blade pressure distributions is unrealistic and has been removed by employing the Van Dyke-Lighthill correction factor.

A set of computations has been performed for the series of 3-bladed propellers for which experimental data were available from NSRDC tests in open water and in the non-uniform inflows due to 3-cycle and 4-cycle screen wakes. The calculated results for the hydrodynamic forces and moments, steady and unsteady, compare well with the experimental values. There is no experimental information on blade pressure distributions for this set of propellers. However, the blade pressure distribution curves in the steady-state case agree qualitatively with experimental curves[18] shown by Mavlyudov (USSR) for a different propeller model (NACA-16, $\bar{a} = 0.8$ mean line section, EAR = 0.95) at 0.8 radius. In the absence of experimentally measured blade pressure distributions for the propellers treated, a comparison is made indirectly through the index of cavitation inception in uniform inflow. It is seen that the predicted values of $\sigma_i = |C_{p_m}|$ are conservative except at the smallest off-design $J = 0.5$ (largest $\Delta J \simeq 0.33$).

The cavitation index $|C_{p_m}|$ reflects the blade pressure in the neighborhood of the leading edge and this is dependent on the correction method for removing the leading edge singularity of the theoretical distribution. However, the observed discrepancies between theory and experiment cannot be attributed solely to the lack of accuracy of the linearized theory when modified by the Van Dyke correction. Experimental determination of the inception of cavitation is dependent on the subjective evaluation of the observer. It is also dependent on the surface finish and accuracy of the propeller model in the immediate vicinity of the leading edge of the blades and on the undissolved air content of the fluid as well. There is a

possibility that flow separation and vortex generation occur near the leading edge and this is not taken into account by the theory. Further studies, both theoretical and experimental, are necessary. The results obtained thus far may be considered reasonable.

REFERENCES

1. W. R. Jacobs and S. Tsakonas, "Generalized Lift Operator Technique for the Solution of the Downwash Integral Equation," DL Report 1308, Stevens Institute of Technology, August 1968; published as "A New Procedure for the Solution of Lifting Surface Problems," J. Hydronautics Vol. 3, No. 1, January 1969.

2. S. Tsakonas, W. R. Jacobs and P. H. Rank, Jr., "Unsteady Propeller Lifting Surface Theory with Finite Number of Chordwise Modes," DL Report 1133, Stevens Institute of Technology, December 1966; J. Ship Research, Vol. 12, No. 1, March 1968.

3. S. Tsakonas, W. R. Jacobs and M. R. Ali, "An Exact Linear Lifting-Surface Theory for a Marine Propeller in a Nonuniform Flow Field," DL Report 1509, Stevens Institute of Technology, February 1972; J. Ship Research Vol. 17, No. 4, December 1973.

4. M. D. Van Dyke, "Second-Order Subsonic Airfoil Theory Including Edge Effects," NACA Report 1274, 1956.

5. M. J. Lighthill, "A New Approach to Thin Aerofoil Theory," Aero. Quart., Vol. 3, pt 3, November 1951.

6. S. Tsakonas and W. R. Jacobs, "Propeller Loading Distributions," DL Report 1319, Stevens Institute of Technology, August 1968; J. Ship Research Vol. 13, No. 4, December 1969.

7. I. H. Abbott and A. E. Von Doenhoff, Theory of Wing Sections , Dover Publications, Inc., New York, 1959.

8. S. F. Hoerner, Fluid-Dynamic Drag, published by the author, 1965.

9. S. Tsakonas and W. R. Jacobs, "Steady and Time-Dependent Propeller Blade Loading and Stress Analysis," Propellers 75 Symposium, Society of Naval Architects and Marine Engineers, July 1975.

10. S. Tsakonas, C. Y. Chen and W. R. Jacobs, "Exact Treatment of the Helicoidal Wake in the Propeller Lifting-Surface Theory," DL Report 1117, Stevens Institute of Technology, August 1966; J. Ship Research Vol. 11, No. 3, September 1967.

11. J. W. Nicholson, "The Approximate Calculations of Bessel Functions of Imaginary Argument," Phil. Mag., Series 6, Vol. 20, December 1910.

REFERENCES

(Continued)

12. L. B. W. Jolley, ed., Summation of Series, Dover Publications, Inc., New York, 1961.

13. J. B. Scarborough, Numerical Mathematical Analysis, The Johns Hopkins Press, Baltimore, Md., 1958.

14. C. E. Watkins, D. S. Woolston and H. J. Cunningham, "A Systematic Kernel Function Procedure for Determining Aerodynamic Forces on Oscillating or Steady Finite Wings at Subsonic Speeds," NASA Technical Report R-48, 1959.

15. S. Tsakonas, J.P. Breslin and M. Miller, "Correlation and Application of an Unsteady Flow Theory for Propeller Forces," Trans. SNAME, Vol.75, 1967.

16. M.L. Miller, "Experimental Determination of Unsteady Propeller Forces," Seventh ONR Symposium on Naval Hydrodynamics, August 1968, pp.255-290.

17. S.B. Denny, "Cavitation and Open Water Performance Tests of a Series of Propellers Designed by Lifting Surface Methods," NSRDC Report 2878, September 1968.

18. M.A. Mavlyudov, "Measurement of Pressure Distribution on the Blades of a Marine Propeller Model," Sbornik Statey po Gidrodinamike Dvirhiteley, "Sudostroyaniye" Publishing House, 1965, pp. 67-72.

19. T.T. Huang and D.E. Hannan, "Pressure Fluctuations in the Regions of Flow Transition," DTNSRDC Report 4723, December 1975.

20. T. Brockett, "Minimum Pressure Envelopes for Modified NACA-66 Sections with NACA a = 0.8 Camber and Buships Type I and Type II Sections," DTMB Report 1780, February 1966.

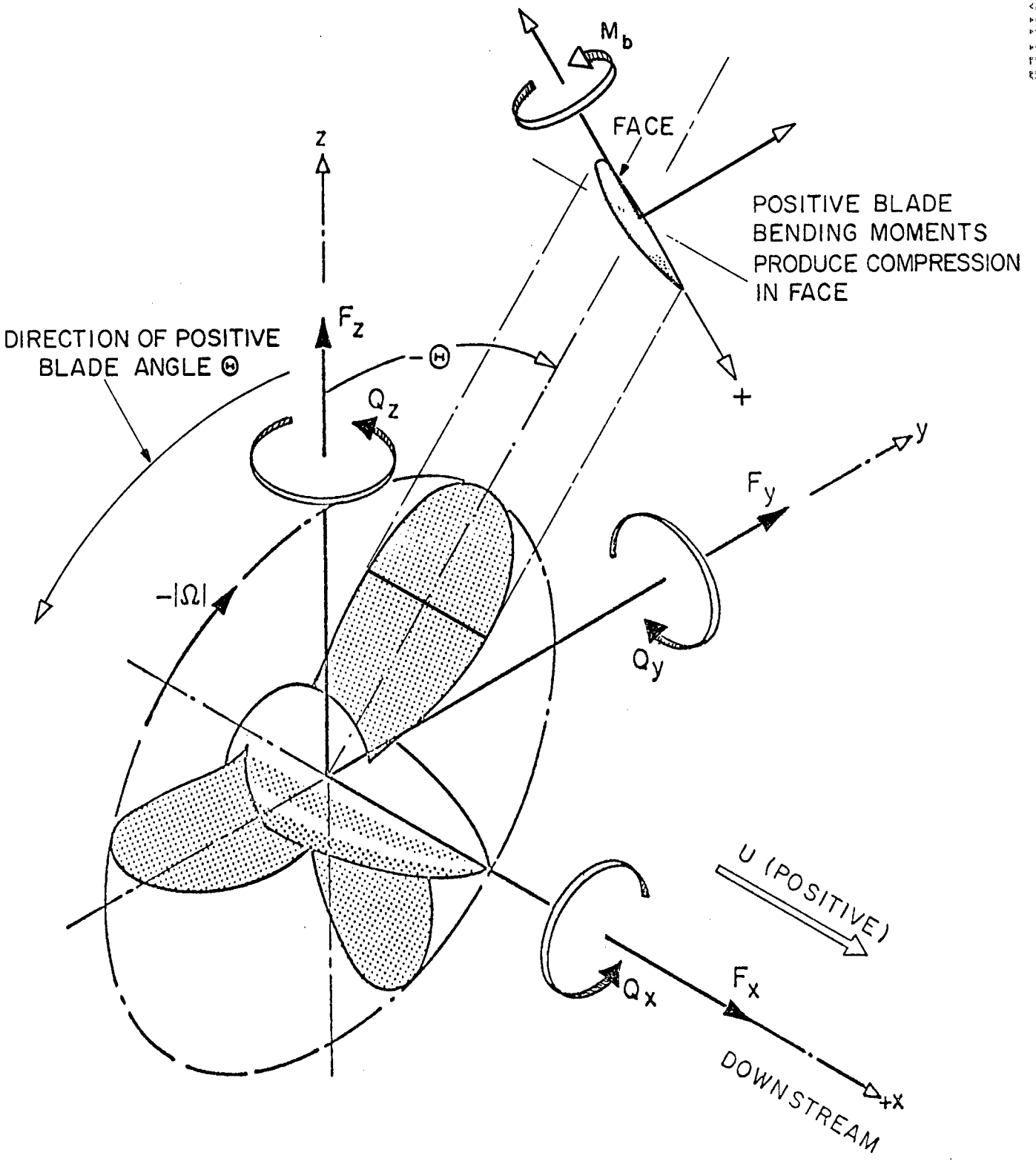

FIG. 1 RESOLUTION OF FORCES AND MOMENTS

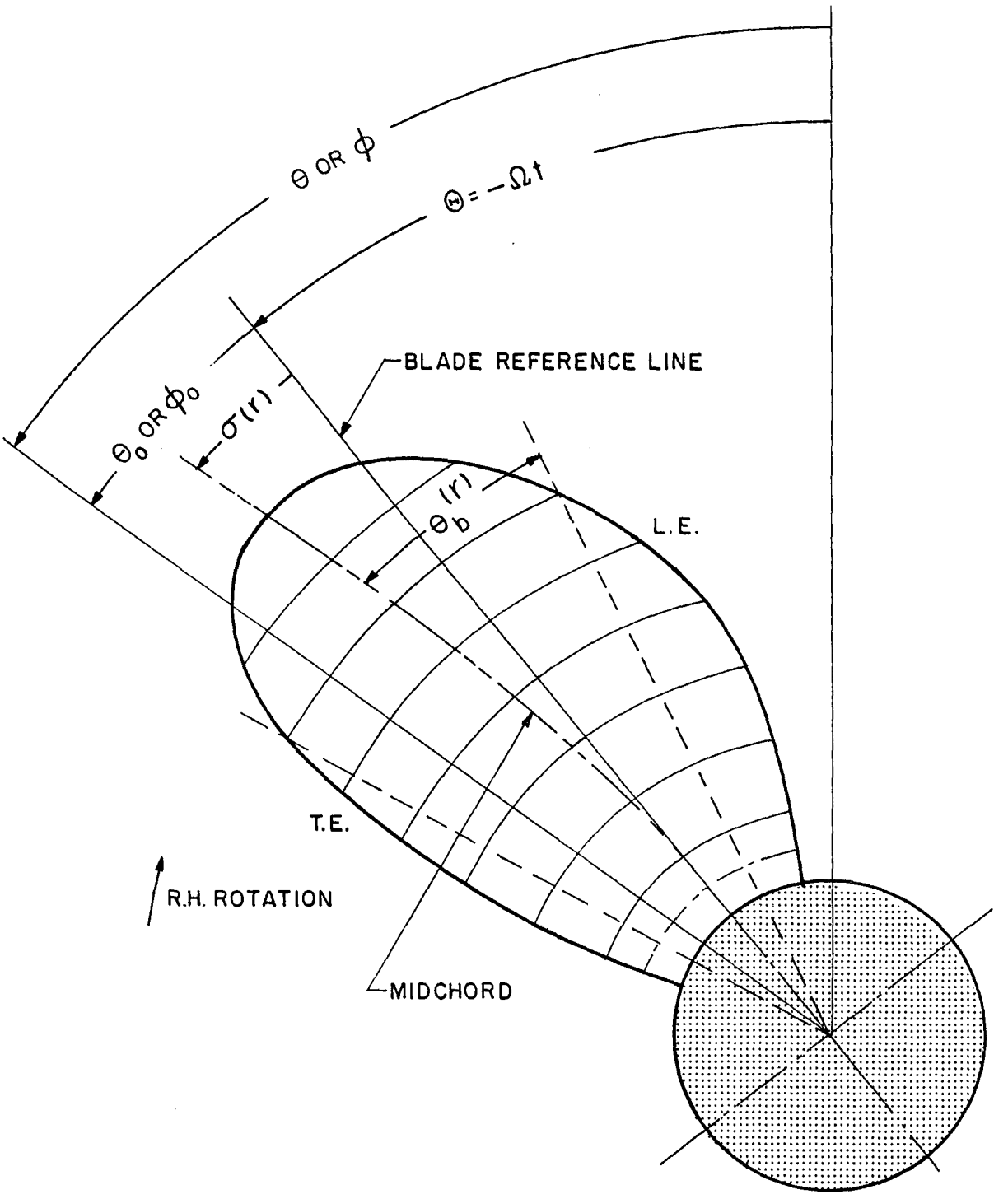

FIG. 2. DEFINITIONS OF ANGULAR MEASURES

NOTE: THE BLADE REFERENCE LINE IS THAT CONNECTING THE SHAFT CENTER WITH THE MIDPOINT OF THE CHORD AT THE HUB

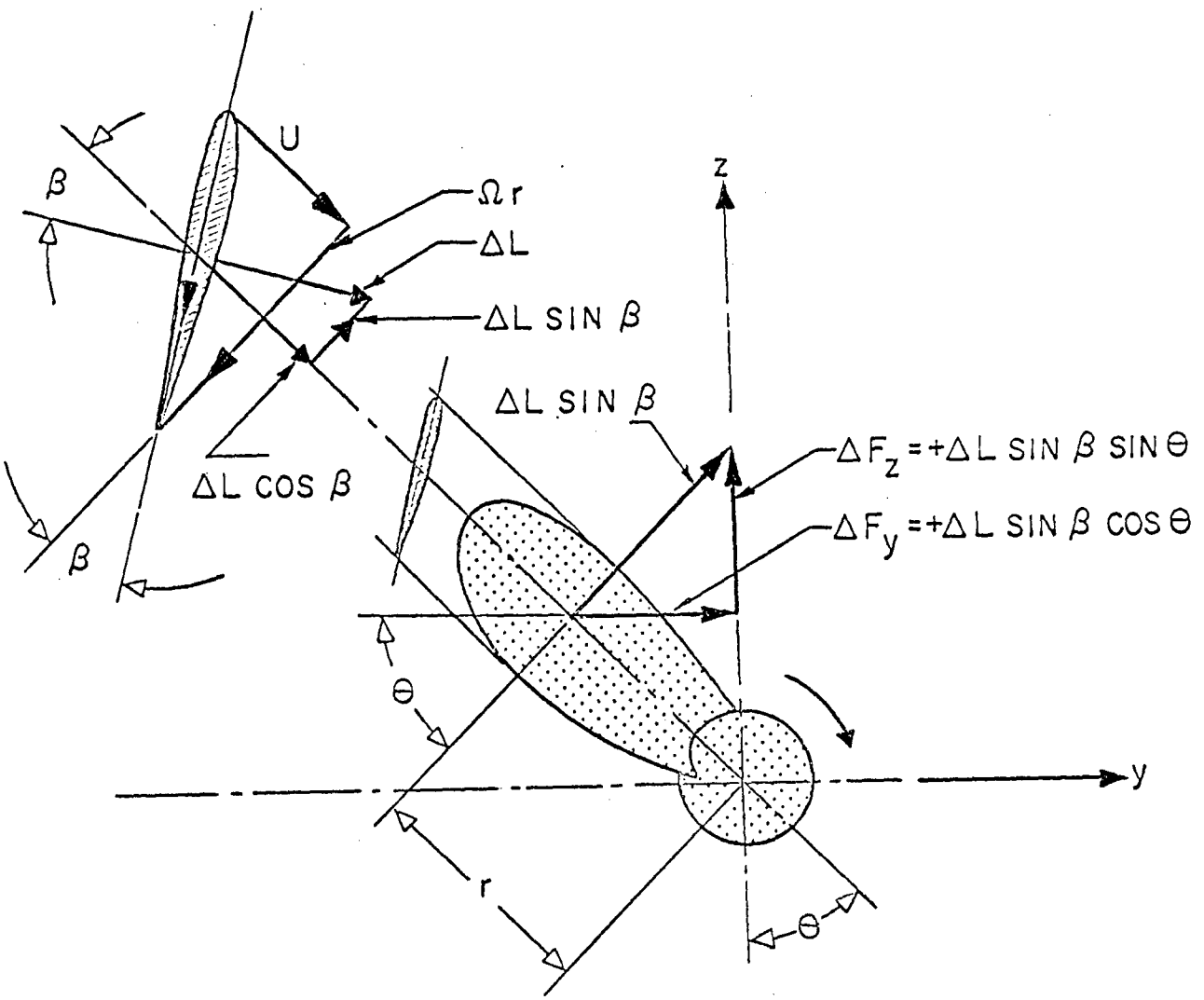

FIG. 3 RESOLUTION OF FORCES

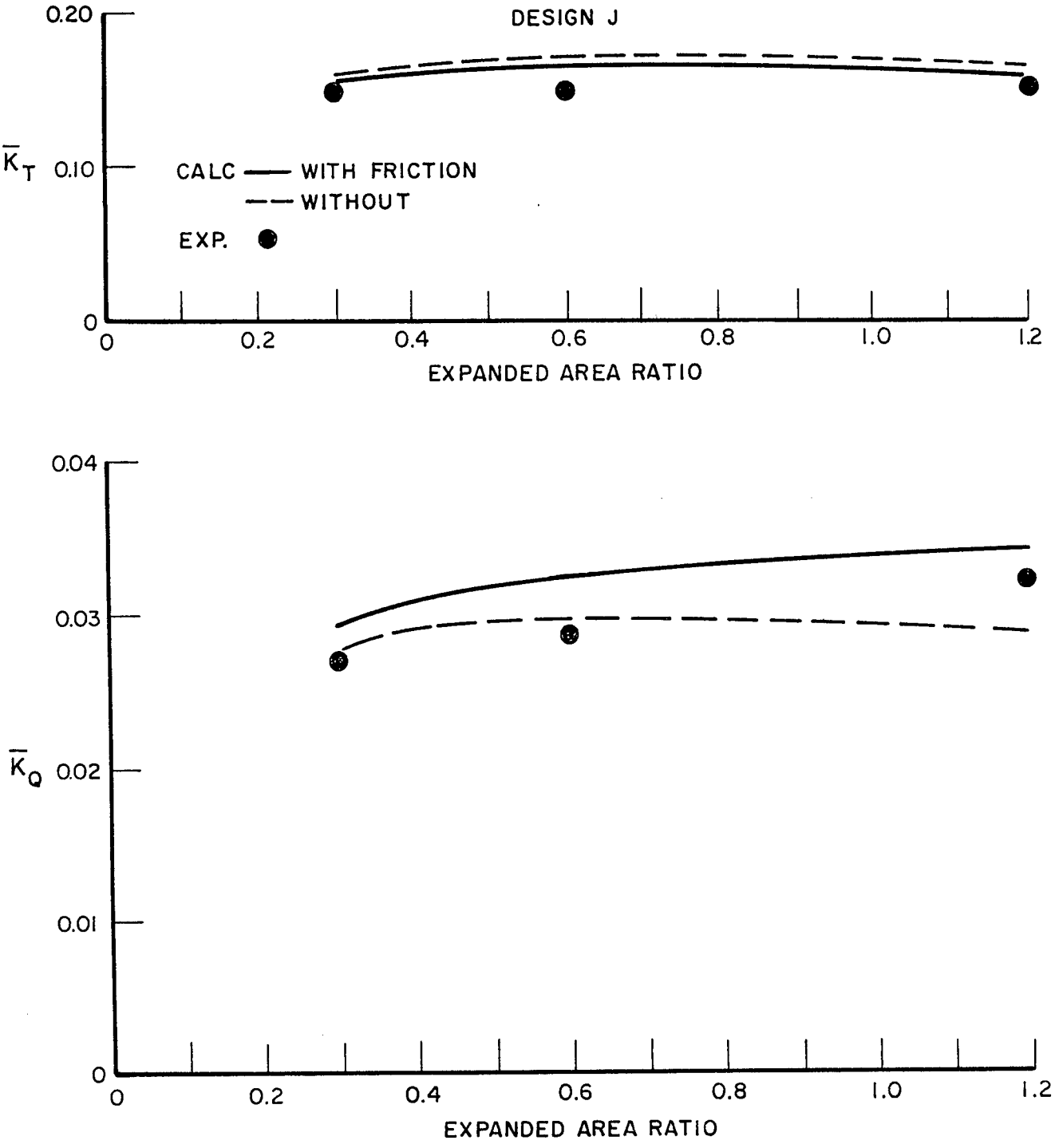

FIG.4. MEAN THRUST AND TORQUE OF DTNSRDC 3-BLADED PROPELLERS AT DESIGN J

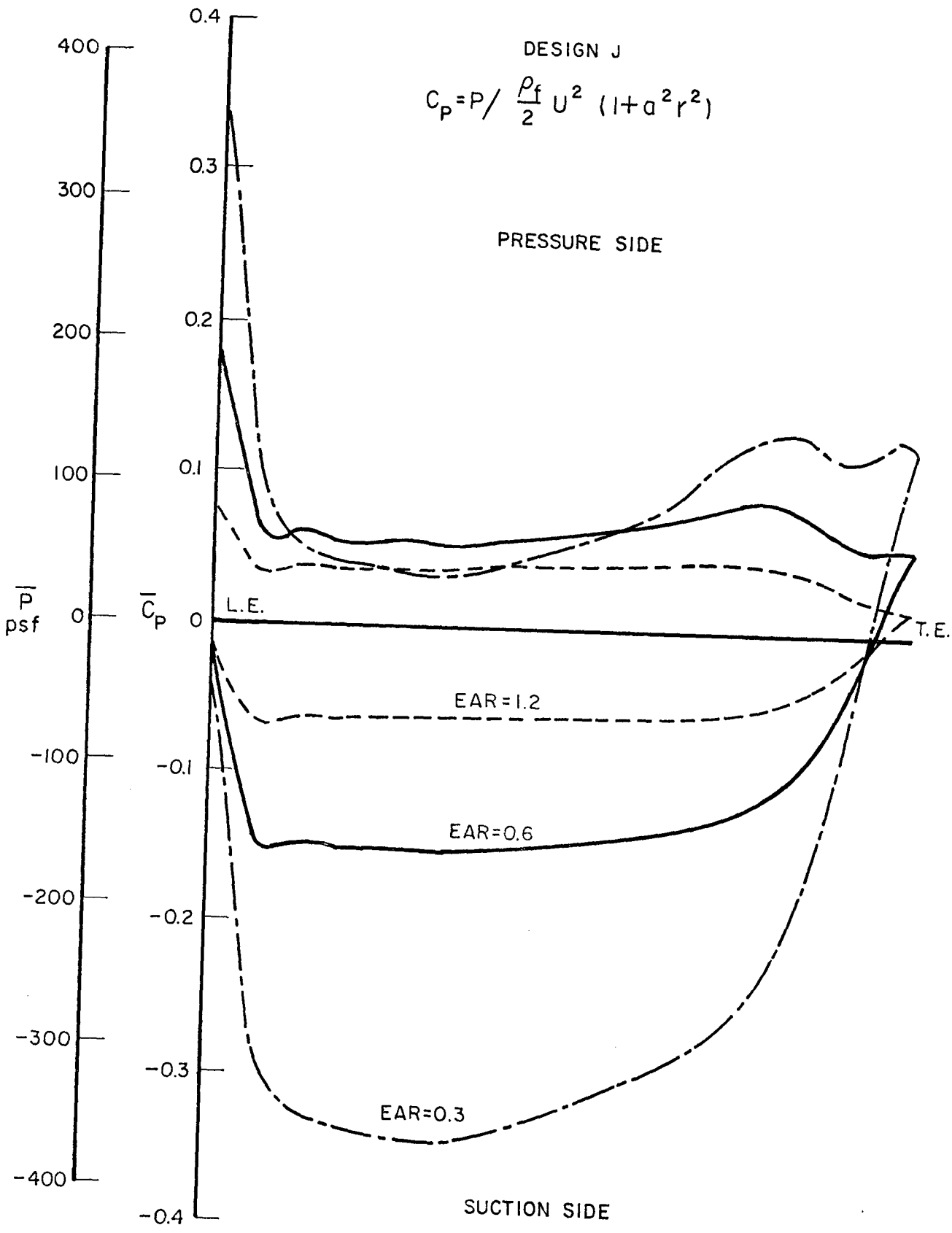

FIG. 5. STEADY-STATE CHORDWISE PRESSURE DISTRIBUTION AT 0.65 RADIUS ON DTNSRDC 3-BLADED PROPELLERS AT DESIGN J.

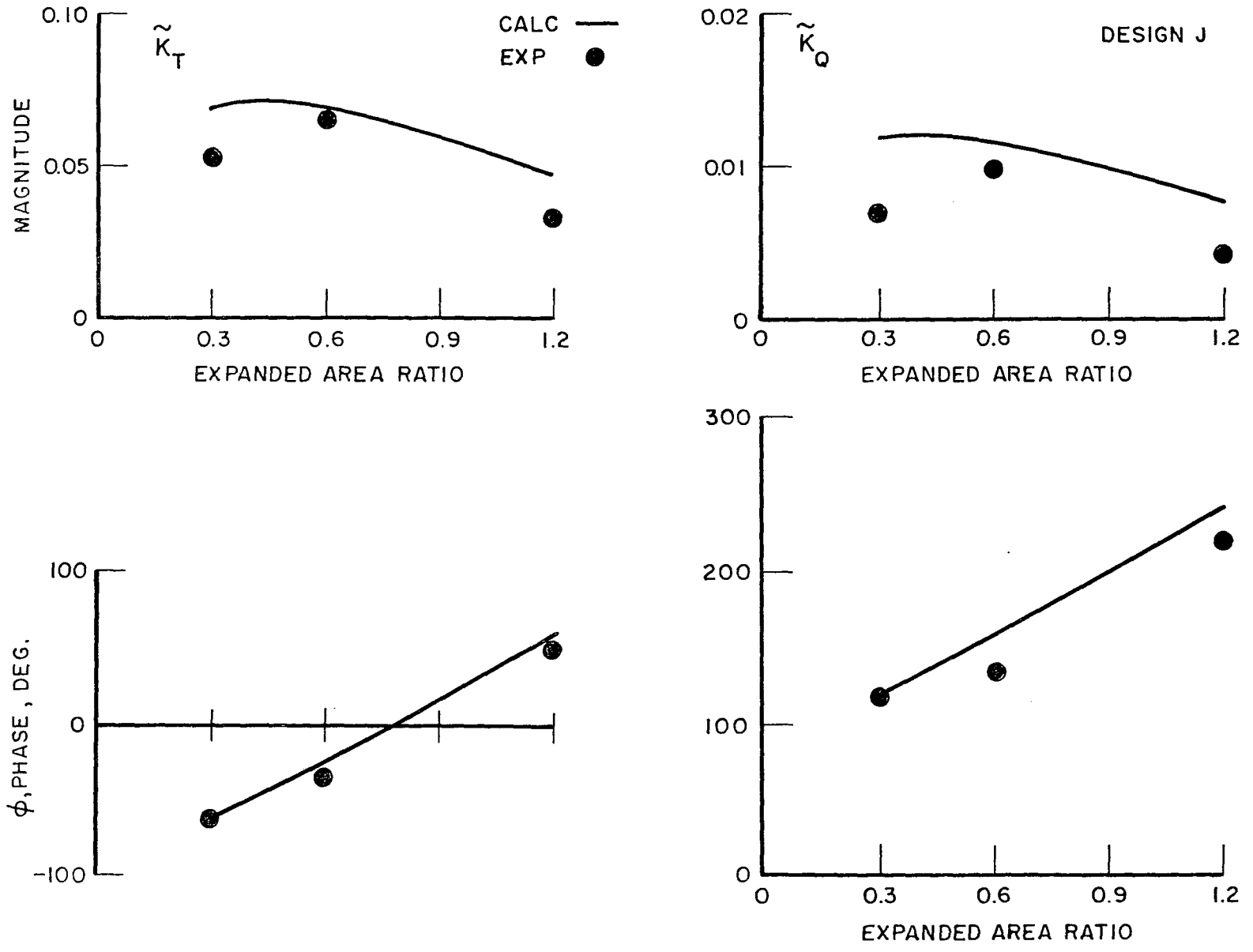

R-1869

FIG.6. BLADE-FREQUENCY THRUST AND TORQUE OF DTNSRDC 3-BLADED PROPELLERS (IN 3-CYCLE SCREEN WAKE)

FOR DL PHASE DEFINITION SEE FIG. 7. (WHERE $\phi/3$ IS SHOWN FOR EAR=0.6)

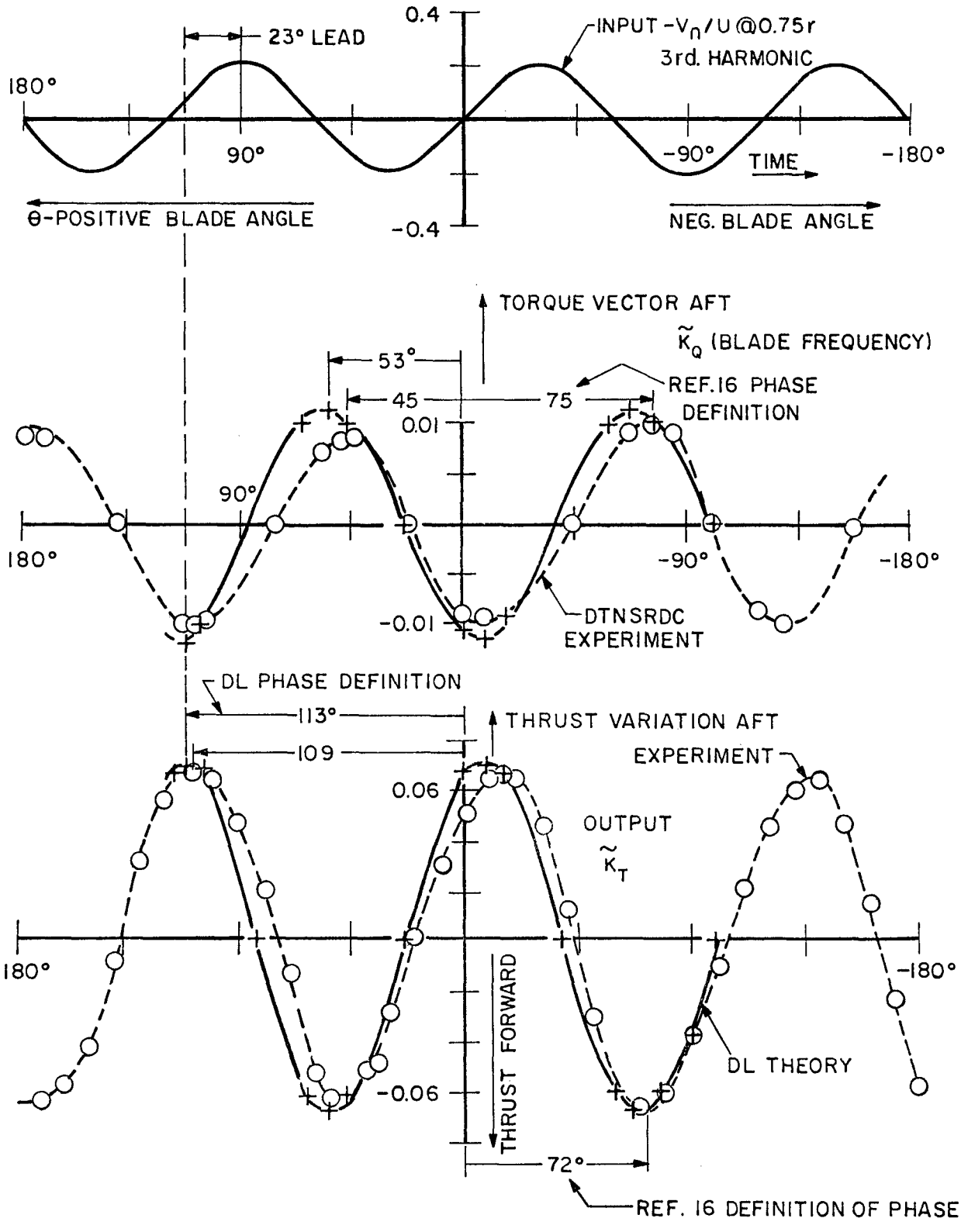

FIG. 7. MEASURED AND CALCULATED BLADE FREQUENCY THRUST AND TORQUE COEFFICIENTS FOR DTNSRDC PROPELLER 4118, EAR=0.6, USING WAKE VALUES OF TABLE V FROM 3-CYCLE SCREEN

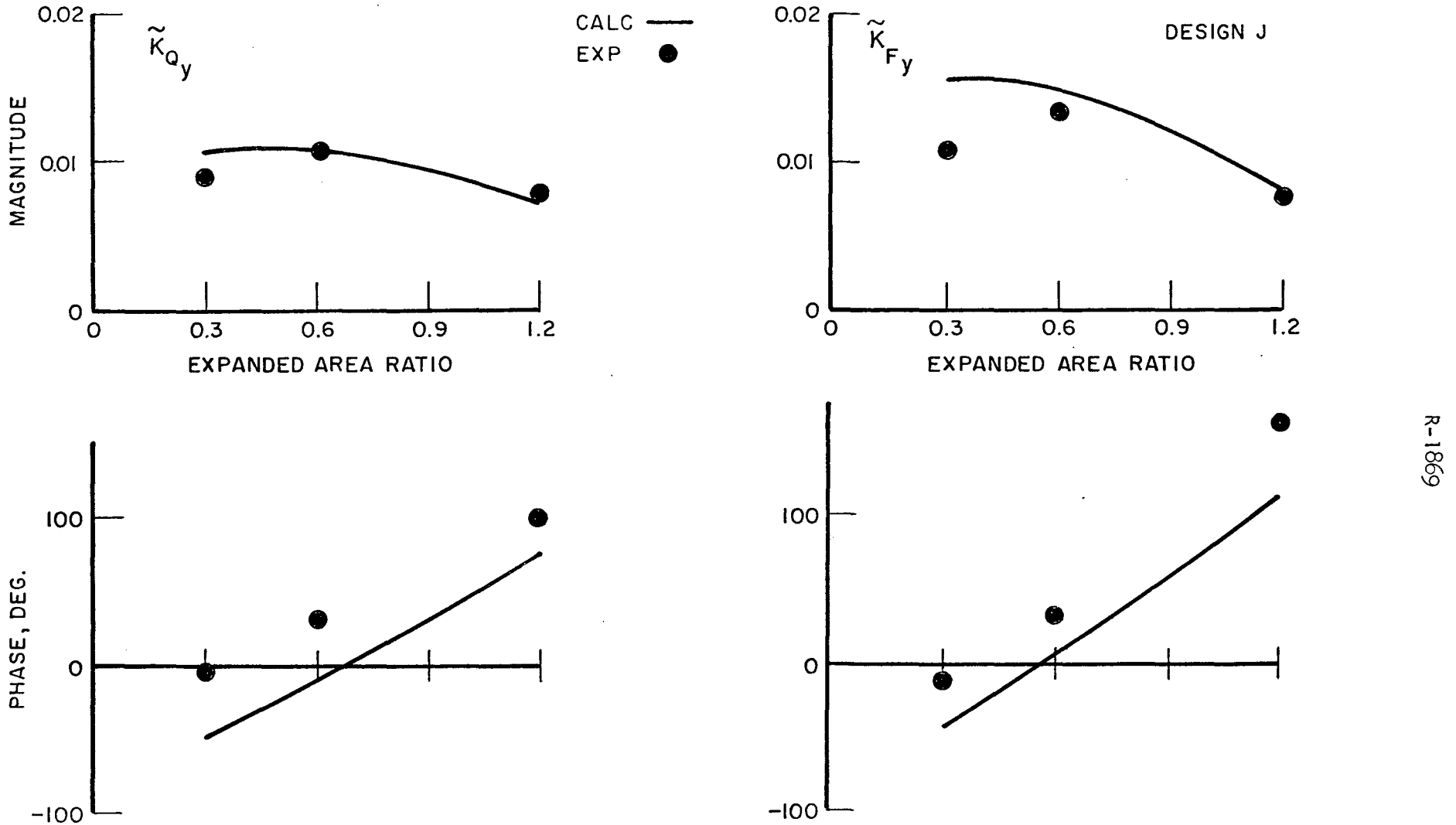

FIG. 8. BLADE-FREQUENCY TRANSVERSE FORCES AND MOMENTS OF DTNSRDC 3-BLADED PROPELLERS (IN 4-CYCLE SCREEN WAKE)

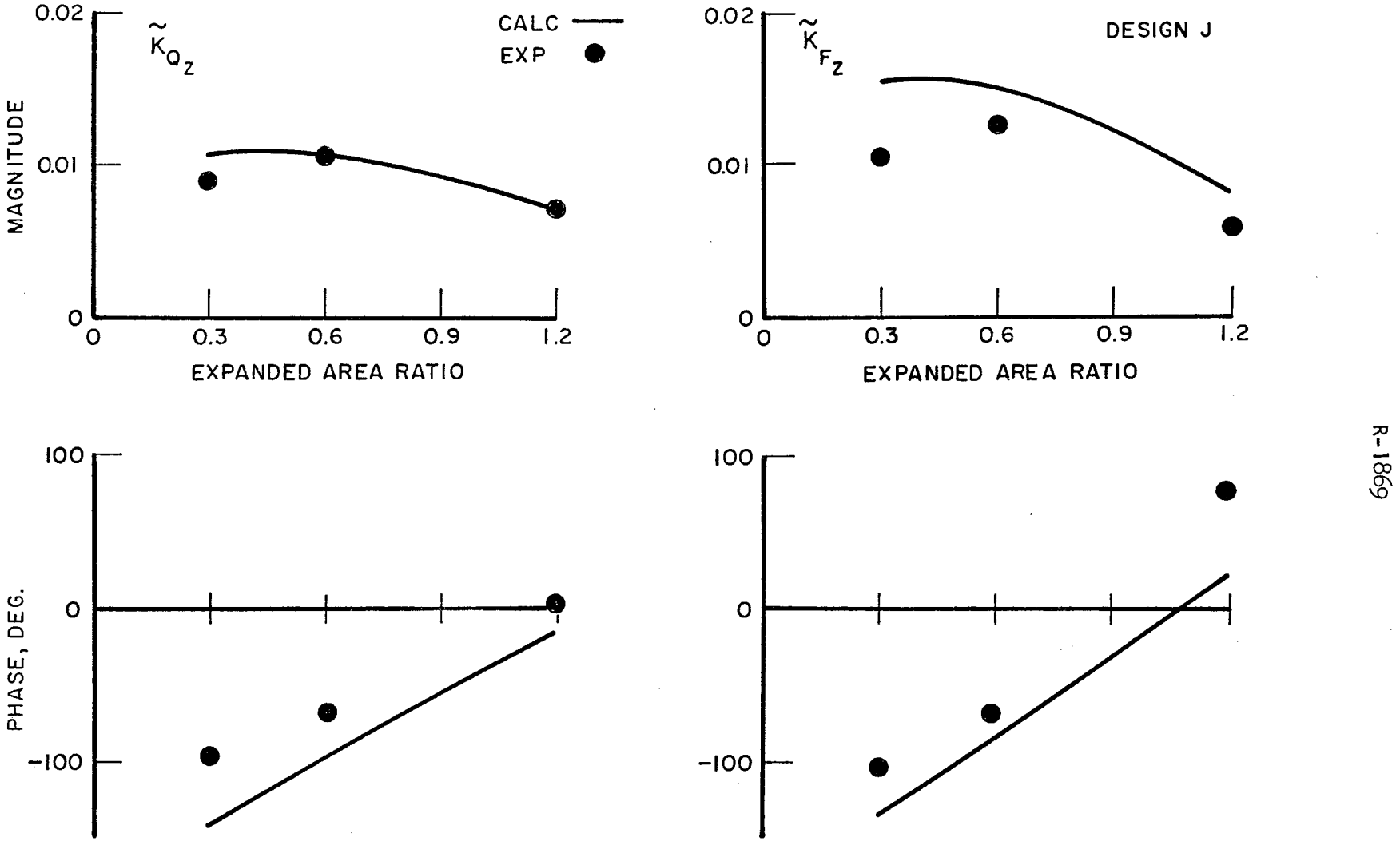

FIG. 9. BLADE-FREQUENCY TRANSVERSE FORCES AND MOMENTS OF DTNSRDC 3-BLADED PROPELLERS (IN 4-CYCLE SCREEN WAKE)

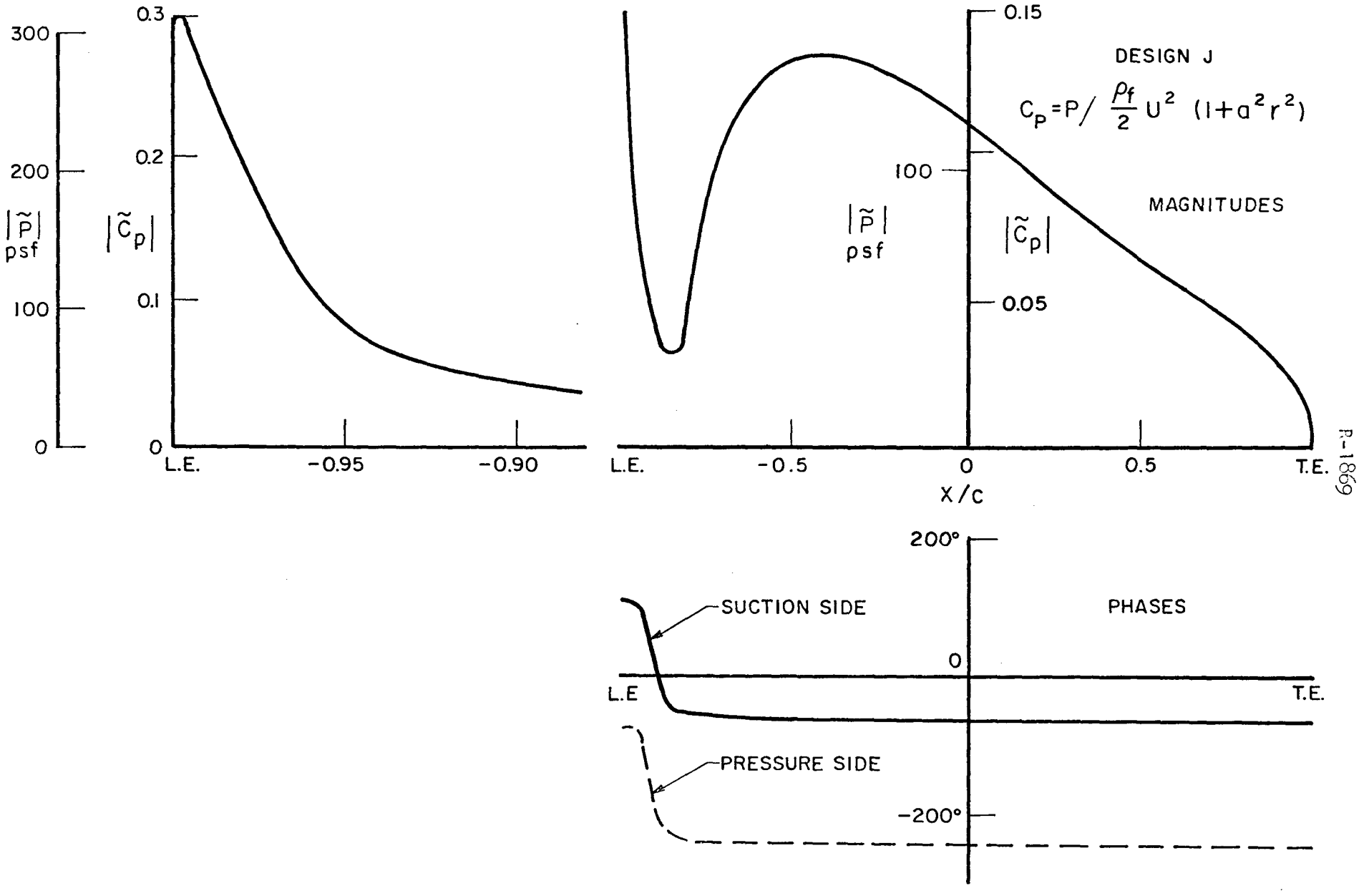

FIG. 10. BLADE-FREQUENCY CHORDWISE PRESSURE DISTRIBUTION ON EACH SIDE OF PROPELLER 4132 (EAR=0.3) AT 0.65 RADIUS

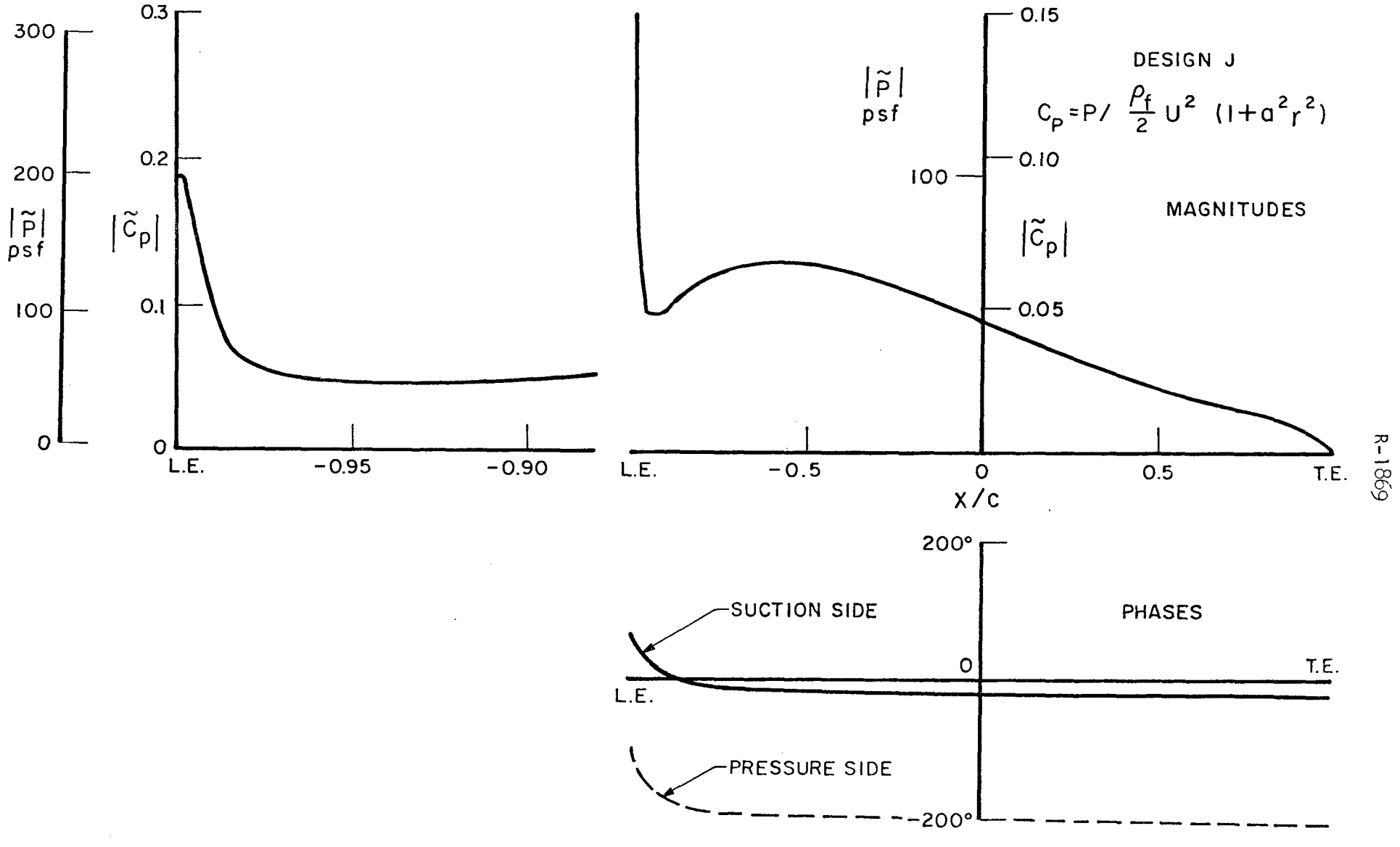

FIG. 11. BLADE-FREQUENCY CHORDWISE PRESSURE DISTRIBUTION ON EACH SIDE OF PROPELLER 4118 (EAR=0.6) AT 0.65 RADIUS

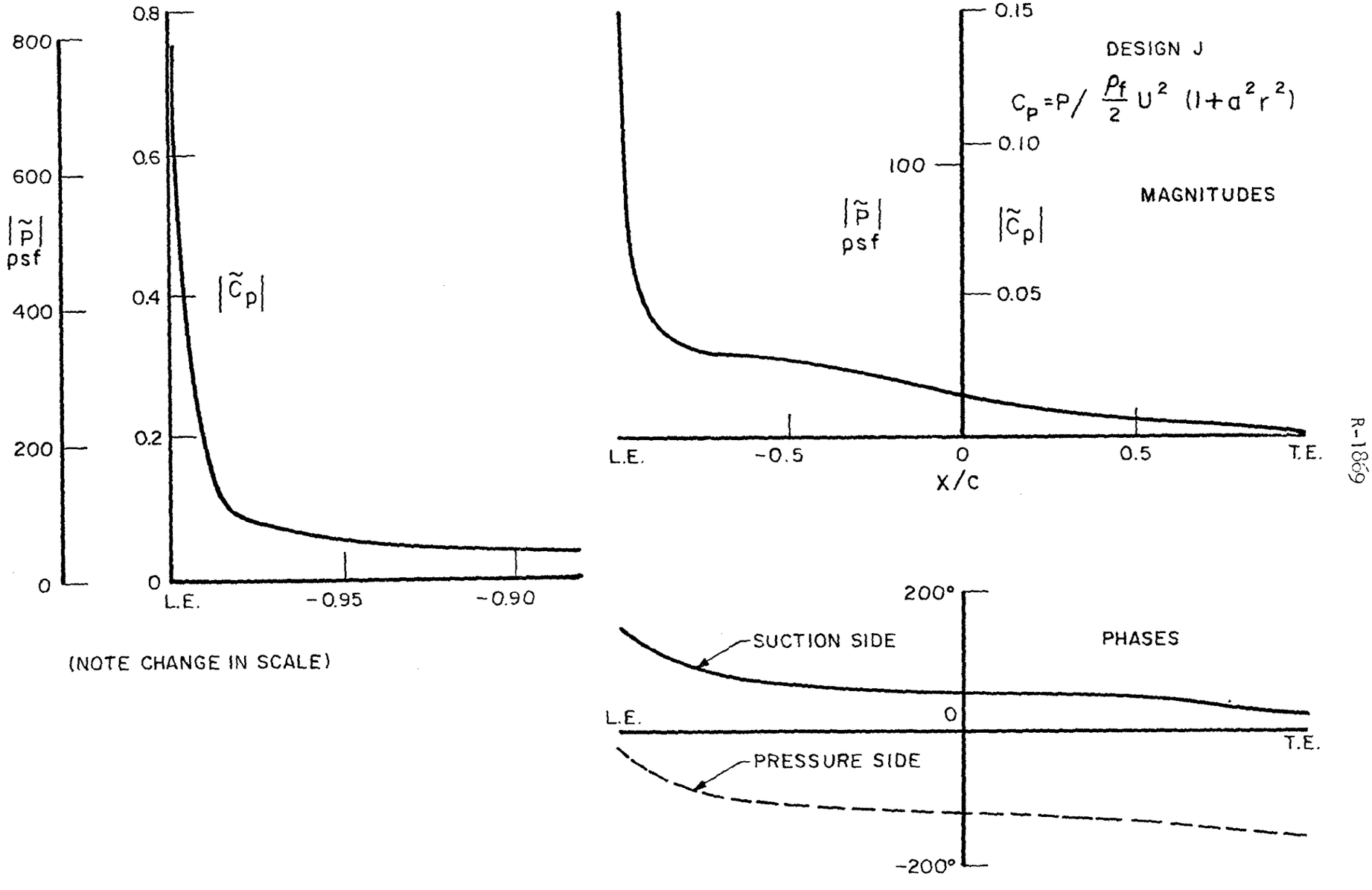

FIG. 12. BLADE-FREQUENCY CHORDWISE PRESSURE DISTRIBUTION ON EACH SIDE OF PROPELLER 4133 (EAR=1.2) AT 0.65 RADIUS

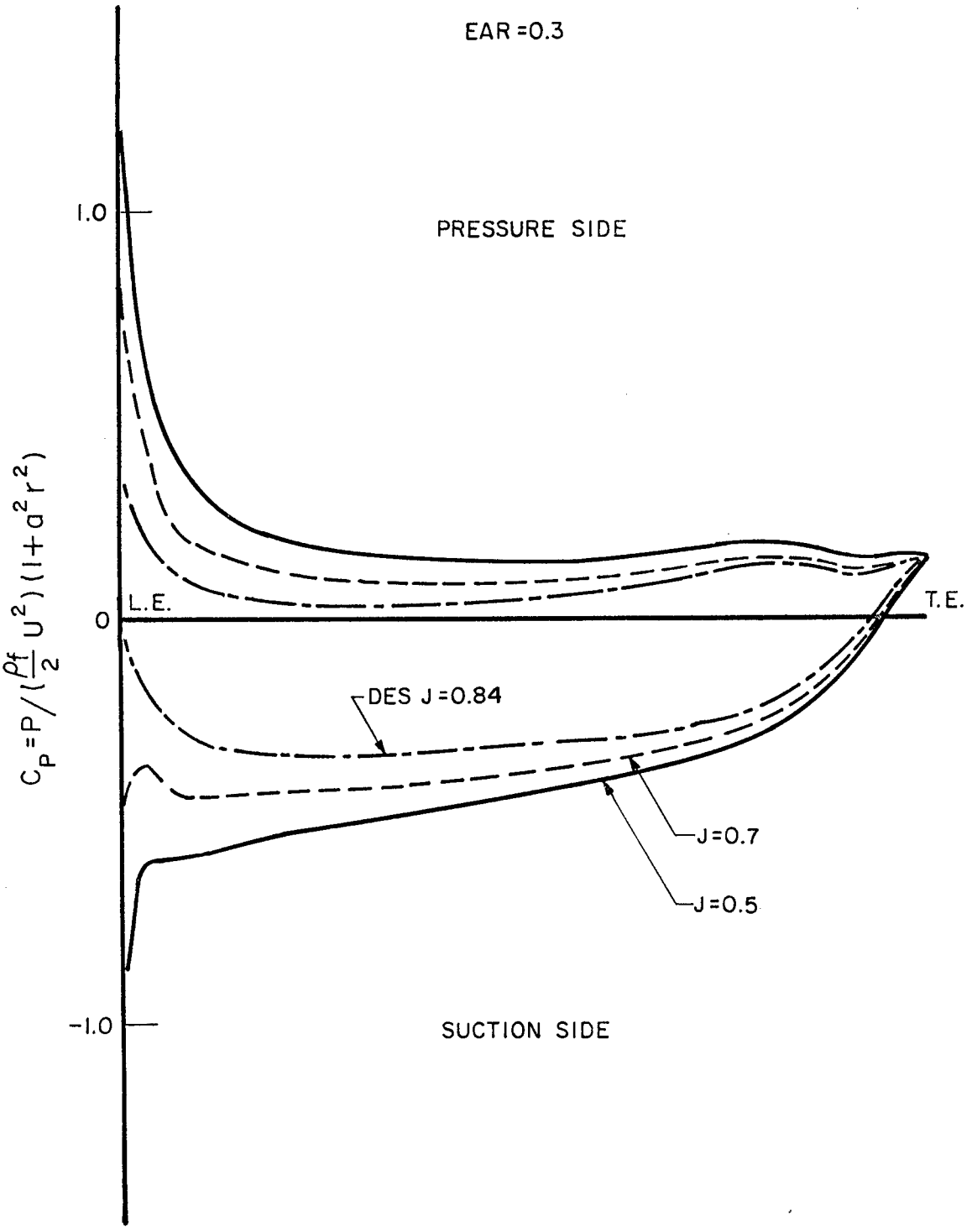

FIG. 13. STEADY-STATE CHORDWISE PRESSURE DISTRIBUTION AT 0.65 RADIUS ON PROPELLER 4132 (EAR=0.3) AT VARIOUS J.

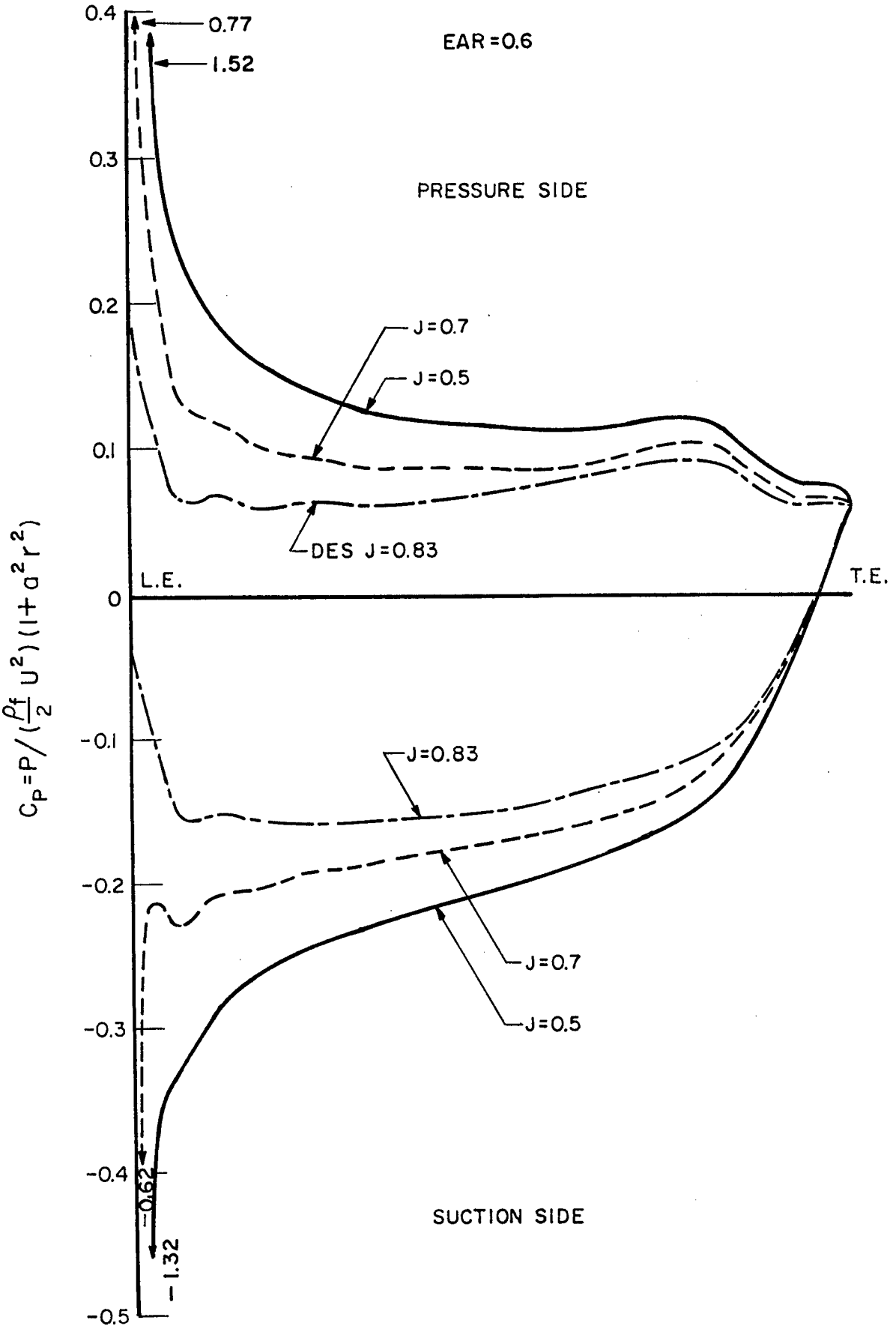

FIG. 14. STEADY-STATE CHORDWISE PRESSURE DISTRIBUTION AT 0.65 RADIUS ON PROPELLER 4118 (EAR=0.6) AT VARIOUS J.

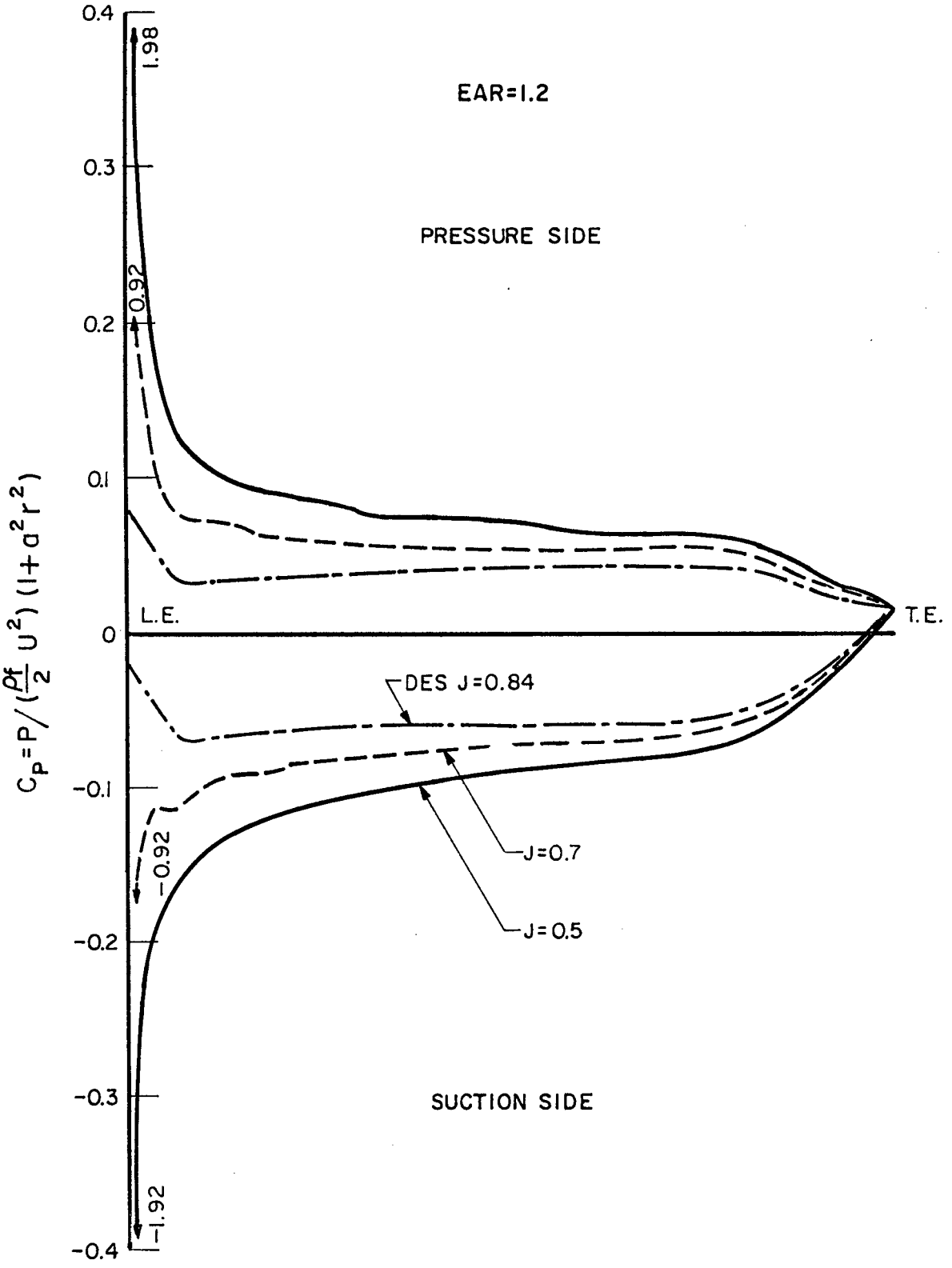

FIG. 15. STEADY-STATE CHORDWISE PRESSURE DISTRIBUTION AT 0.65 RADIUS ON PROPELLER 4133 (EAR=1.2) AT VARIOUS J.

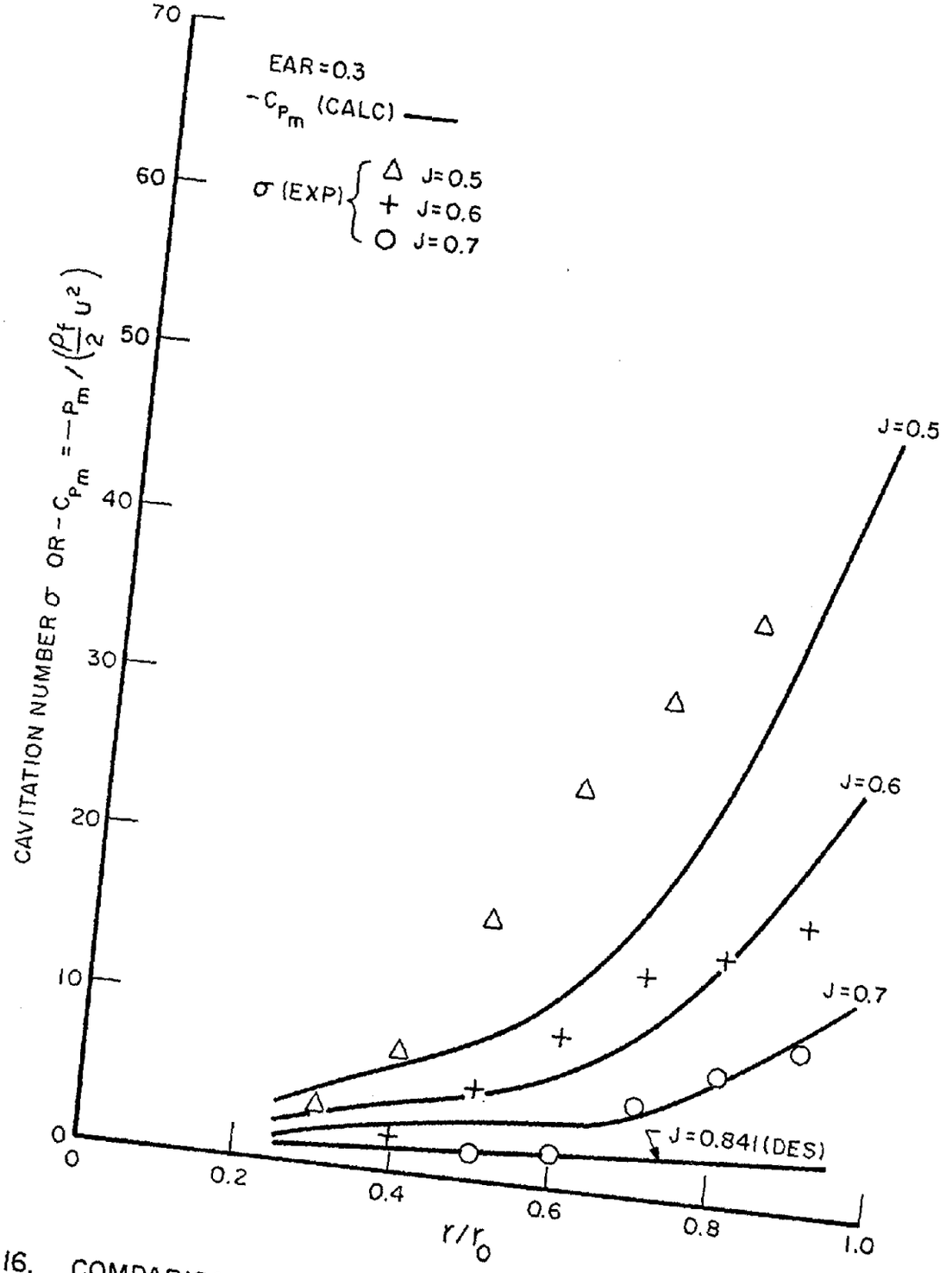

FIG. 16. COMPARISON OF CALCULATED $-C_{P_{min}}$ AND EXPERIMENTAL CAVITATION NUMBER σ, PROPELLER 4132 (EAR = 0.3)

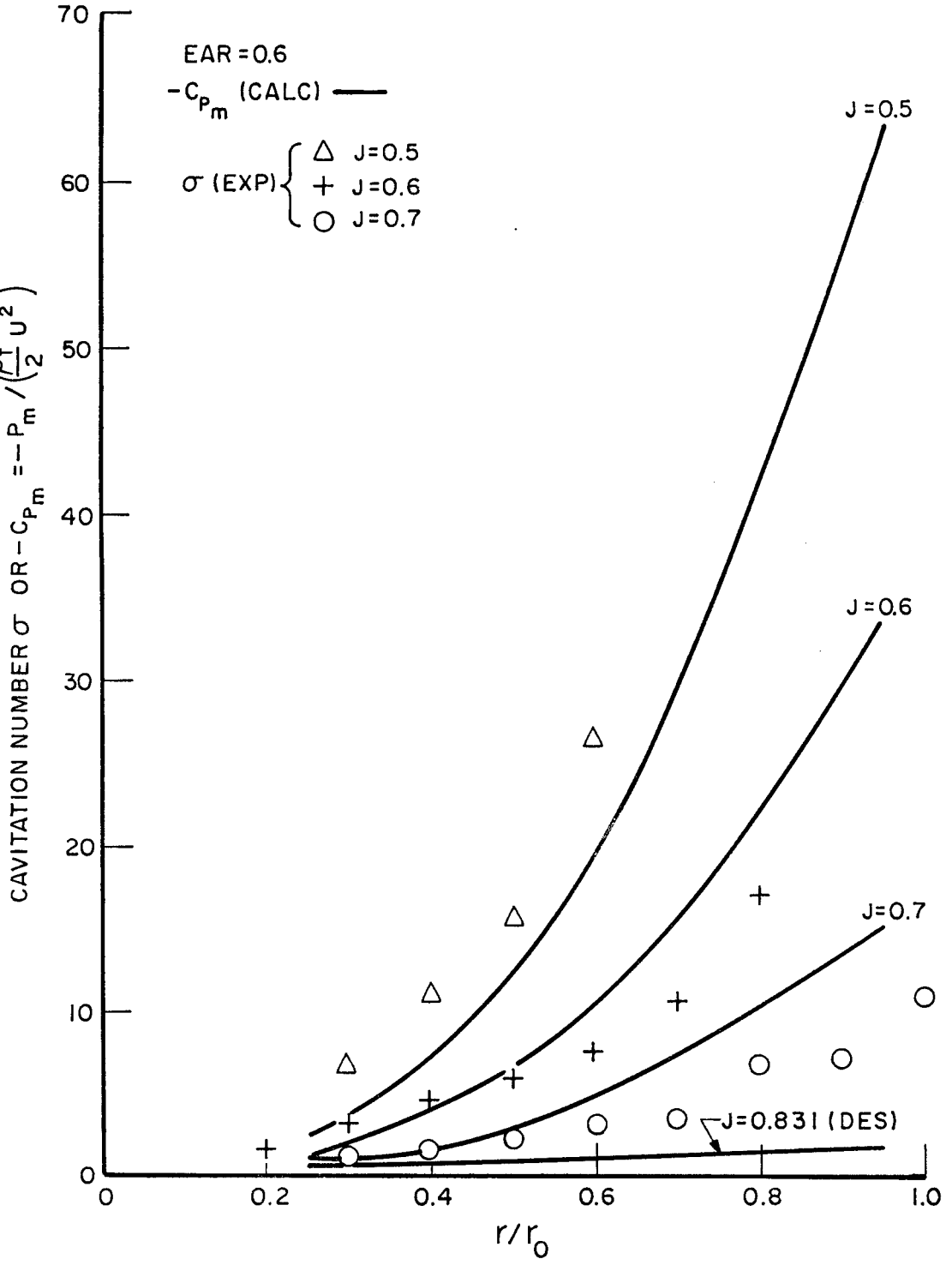

FIG. 17. COMPARISON OF CALCULATED $-C_{P_{min}}$ AND EXPERIMENTAL CAVITATION NUMBER σ, PROPELLER 4118 (EAR = 0.6)

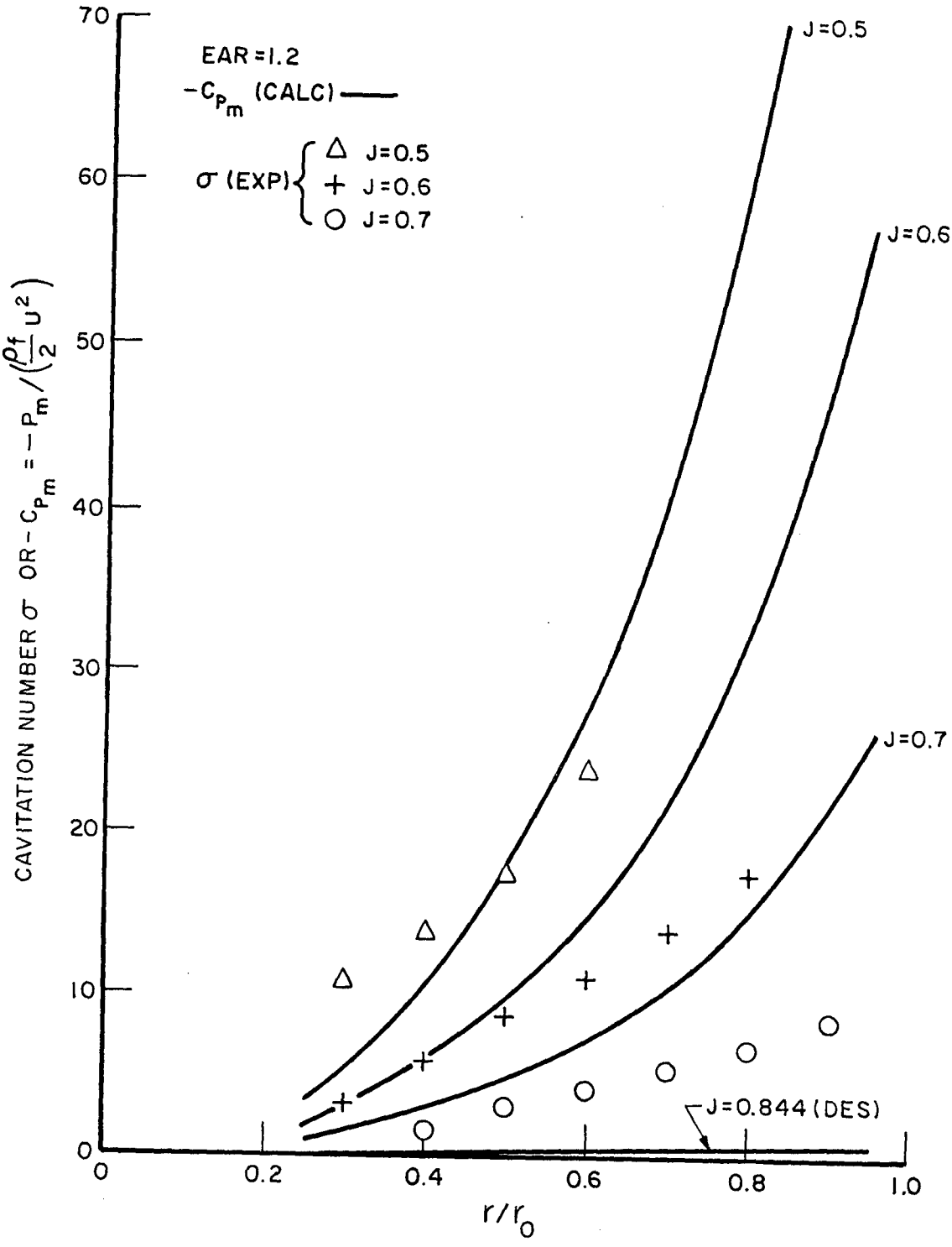

FIG. 18. COMPARISON OF CALCULATED $-C_{P_{min}}$ AND EXPERIMENTAL CAVITATION NUMBER σ, PROPELLER 4133 (EAR = 1.2)

APPENDIX A

1. Evaluation of the φ_α- and θ_α- Integrals of the Integral Equation (19)

1) $$I^{(\bar{m})}(y) = \frac{1}{\pi}\int_0^{\pi} \Phi(\bar{m}) e^{iy\cos\varphi}\, d\varphi$$

$$I^{(1)}(y) = \frac{1}{\pi}\int_0^{\pi} (1-\cos\varphi)\, e^{iy\cos\varphi}\, d\varphi = J_o(y) - iJ_1(y)$$

$$I^{(2)}(y) = \frac{1}{\pi}\int_0^{\pi} (1+2\cos\varphi)\, e^{iy\cos\varphi}\, d\varphi = J_o(y) + i2J_1(y)$$

$$I^{(\bar{m}>2)}(y) = \frac{1}{\pi}\int_0^{\pi} \cos(\bar{m}-1)\varphi\, e^{iy\cos\varphi}\, d\varphi = i^{\bar{m}-1} J_{\bar{m}-1}(y)$$

where $J_n(y)$ is the Bessel function of the first kind of order n and argument y

2) $$\Lambda^{(n)}(z) = \int_0^{\pi} \Theta(\bar{n})\, e^{-iz\cos\theta} \sin\theta\, d\theta$$

a) Birnbaum distribution

$$\Lambda^{(1)}(z) = \frac{1}{\pi}\int_0^{\pi} \cot\frac{\theta}{2}\, e^{-iz\cos\theta}\sin\theta\, d\theta = J_o(z) - iJ_1(z)$$

$$\Lambda^{(\bar{n}>1)}(z) = \frac{1}{\pi}\int_0^{\pi} \sin(\bar{n}-1)\theta\, \sin\theta\, e^{-iz\cos\theta}\, d\theta$$

$$= \frac{(-i)^{\bar{n}-2}}{2}\left[J_{\bar{n}-2}(z) + J_{\bar{n}}(z)\right]$$

b) "Roof-top" distribution ($\bar{a}$ mean lines)

$$\Lambda^{(1)}(z) = \int_0^{\cos^{-1}(1-2\bar{a})} e^{-iz\cos\theta} \sin\theta\, d\theta$$

$$+ \int_{\cos^{-1}(1-2\bar{a})}^{\pi} \frac{(1+\cos\theta)}{2(1-\bar{a})}\, e^{-iz\cos\theta} \sin\theta\, d\theta$$

$$= e^{-iz}\left\{\frac{i}{z} + \frac{1}{2(1-\bar{a})z^2}\left[e^{i2\bar{a}z} - e^{i2z}\right]\right\}$$

(For $\bar{a} = 1$, $\Lambda^{(1)}(z) = \frac{2 \sin z}{z}$.)

$$\Lambda^{(\bar{n}>1)}(z) = 0$$

c) Sine series distribution

$$\Lambda^{(n)}(z) = \frac{1}{\pi} \int_0^{\pi} \sin \bar{n}\theta \sin\theta \, e^{-iz\cos\theta} \, d\theta$$

$$= \frac{(-i)^{\bar{n}-1}}{2} \left[J_{\bar{n}-1}(z) + J_{\bar{n}+1}(z) \right]$$

II. Functions Required for Evaluating the Integrand of the Kernel Function at the Singularity (see Reference 3) and the Propeller-generated Moments (see section A,4)

1) $$I_1^{(\bar{m})}(y) = \frac{1}{\pi} \int_0^{\pi} \Phi(\bar{m}) \, e^{iy\cos\varphi} \cos\varphi \, d\varphi$$

$$I_1^{(1)}(y) = -\frac{1}{2} \left[J_o(y) - J_2(y) \right] + iJ_1(y)$$

$$I_1^{(2)}(y) = \left[J_o(y) - J_2(y) \right] + iJ_1(y)$$

$$I_1^{(\bar{m}>2)}(y) = \frac{i^{\bar{m}-2}}{2} \left[-J_{\bar{m}}(y) + J_{\bar{m}-2}(y) \right]$$

2) $$\Lambda_1^{\bar{m}}(z) = \int_0^{\pi} \Theta(\bar{n}) \sin\theta \cos\theta \, e^{-iz\cos\theta} \, d\theta$$

a) Birnbaum distribution

$$\Lambda_1^{(1)}(z) = \frac{1}{2} \left[J_o(z) - J_2(z) \right] - iJ_1(z)$$

$$\Lambda_1^{(\bar{n}>1)}(z) = \frac{(-i)^{\bar{n}+1}}{4} \left[J_{\bar{n}-3}(z) - J_{\bar{n}+1}(z) \right]$$

b) "Roof-top distribution ($\bar{a}$ mean lines)

$$\Lambda_1^{(1)}(z) = e^{-iz} \left\{ \frac{i}{z} + \frac{1}{z^2} + \frac{1}{z^2(1-\bar{a})} \left[\frac{(1-2\bar{a}}{2} - \frac{i}{z} \right) e^{i2\bar{a}z} + \left(\frac{1}{2} + \frac{i}{z} \right) e^{i2z} \right] \right\}$$

(For $\bar{a} = 1$, $\Lambda_1^{(1)}(z) = \frac{i2}{z}\left(\cos z - \frac{\sin z}{z}\right)$.)

c) Sine series distribution

$$\Lambda_1^{(\bar{n})}(z) = \frac{(-i)^{\bar{n}+2}}{4}\left[J_{\bar{n}-2}(z) - J_{\bar{n}+2}(z)\right]$$

It is to be noted that the values for negative argument, i.e., $I^{(\bar{m})}(-y)$, $I_1^{(\bar{m})}(-y)$, $\Lambda^{(\bar{n})}(-z)$ and $\Lambda_1^{(\bar{n})}(-z)$, are the conjugates of the values given above.

APPENDIX B

TABLE OF INTEGRALS OF EQUATION (33)

1) $$\int_0^{\pi} e^{\pm i\lambda\cos\theta} \sin\theta d\theta = \frac{2}{\lambda}\sin\lambda = 2G(\lambda) \qquad (=2 \text{ when } \lambda = 0)$$

2) $$\int_0^{\pi} e^{\pm i\lambda\cos\theta} \sin 2\theta d\theta = \pm\frac{4i}{\lambda}\left(\frac{\sin\lambda}{\lambda} - \cos\lambda\right) = \pm 4iF(\lambda) \qquad (=0 \text{ when } \lambda=0)$$

3) $$\int_0^{\pi} e^{\pm i\lambda\cos\theta} \sin 3\theta d\theta = \frac{2}{\lambda}\left\{\sin\lambda\left(3 - \frac{8}{\lambda^2}\right) + \frac{8}{\lambda}\cos\lambda\right\} = 6G(\lambda) - \frac{16}{\lambda}F(\lambda)$$

$$(=2/3 \text{ when } \lambda=0)$$

4) $$\int_0^{\pi} e^{\pm i\lambda\cos\theta} \sin 4\theta d\theta = \pm\frac{8i}{\lambda}\left\{\frac{\sin\lambda}{\lambda}\left(5 - \frac{12}{\lambda^2}\right) + \cos\lambda\left(\frac{12}{\lambda^2} - 1\right)\right\}$$

$$= \pm\frac{8i}{\lambda}\left\{4G(\lambda) + \left(\lambda - \frac{12}{\lambda}\right)F(\lambda)\right\} \qquad (=0 \text{ when } \lambda=0)$$

5) $$\int_0^{\pi} e^{\pm i\lambda\cos\theta} \cos\frac{\theta}{2} d\theta = 2J_0(\lambda) - 4\sum_{n=1}^{\infty}\frac{(-1)^n J_{2n}(\lambda)}{(4n+1)(4n-1)} \mp 4i\sum_{n=1}^{\infty}\frac{(-1)^n J_{2n-1}(\lambda)}{(4n-1)(4n-3)}$$

$$= B(\pm\lambda) \qquad (=2 \text{ when } \lambda=0)$$

(Three or four terms of this series are sufficient.)

APPENDIX C

RESOLUTION OF FORCES AND MOMENTS

With the present coordinate system and sign convention (see Figures 1 to 3) the propeller, its N blades rotating with angular velocity $-\Omega$, is assumed to lie on a helicoidal surface given by

$$F(x,y,z) = x + \frac{1}{a} \tan^{-1} \frac{y}{z} = 0 \qquad \text{(C-1)}$$

where in cylindrical coordinates

$$x = \varphi_o/a$$

$$y = -r \sin\theta$$

$$z = r \cos\theta$$

$$\theta = \varphi_o - \Omega t + \bar{\theta}_n$$

The unit normal to this surface has components

$$\bar{n} = \frac{F_x, F_y, F_z}{\sqrt{F_x^2 + F_y^2 + F_z^2}} = \frac{1, z/ar^2, -y/ar^2}{\sqrt{1+a^2r^2}/ar} \qquad \text{(C-2)}$$

so that

$$n_x = \frac{ar}{\sqrt{1 + a^2 r^2}} = \cos\beta$$

$$n_y = \frac{z/r}{\sqrt{1 + a^2 r^2}} = \sin\beta \cos\theta$$

$$n_z = \frac{-y/r}{\sqrt{1 + a^2 r^2}} = \sin\beta \sin\theta$$

where $\beta = \tan^{-1} \frac{1}{ar}$, the hydrodynamic pitch angle.

The elemental forces are then

$$\Delta F_x = \Delta P \cos\beta \, \Delta S$$

$$\Delta F_y = \Delta P \sin\beta \cos(\Omega t - \varphi_o - \bar{\theta}_n) \, \Delta S \qquad \text{(C-3)}$$

$$\Delta F_z = -\Delta P \sin\beta \sin(\Omega t - \varphi_o - \theta_n) \, \Delta S$$

The elemental moments can be expressed as

$$\vec{\Delta Q} = \begin{vmatrix} i & j & k \\ x & y & z \\ n_x & n_y & n_z \end{vmatrix} (\Delta P)(\Delta S) \qquad \text{(C-4)}$$

so that

$$\Delta Q_x = \Delta P(yn_z - zn_y) \, \Delta S = -\Delta P \, r\sin\beta \, \Delta S$$

$$\Delta Q_y = -\Delta P(xn_z - zn_x) \, \Delta S$$

$$= \Delta P \cdot r \left[\varphi_o \tan\beta \sin\beta \sin(\Omega t - \varphi_o - \bar{\theta}_n) + \cos\beta \cos(\Omega t - \varphi_o - \bar{\theta}_n)\right] \Delta S$$

$$\Delta Q_z = \Delta P(xn_y - yn_x) \, \Delta S$$

$$= \Delta P \cdot r \left[\varphi_o \tan\beta \sin\beta \cos(\Omega t - \varphi_o - \bar{\theta}_n) - \cos\beta \sin(\Omega t - \varphi_o - \bar{\theta}_n)\right] \Delta S$$

The total force in the x-direction (thrust) is

$$F_x = \mathrm{Re} \sum_{n=1}^{N} e^{iq(\Omega t - \bar{\theta}_n)} \int_S \int \Delta P^{(q)}(r, \varphi_o) \cos\beta(r) \, dS$$

Since $dS = r\,dr\,d\varphi_o = r\theta_b^r \sin\varphi_\alpha \, d\varphi_\alpha \, dr$, $0 \le \varphi_\alpha \le \pi$

$$L^{(q)}(r, \varphi_\alpha) = \Delta P^{(q)}(r, \varphi_o) \; r \; \theta_b^r$$

and $$\sum_{n=1}^{N} e^{\pm iq\bar{\theta}_n} = \begin{cases} N \text{ for } q = \ell N, \; \ell = 0, 1, 2, \ldots \\ 0 \text{ otherwise} \end{cases}$$

$$F_x = \mathrm{Re}\left\{N\, e^{i\ell N\Omega t} \int_0^{\pi}\int_r L^{(\ell N)}(r,\varphi_\alpha)\cos\beta(r)\,\sin\varphi_\alpha\, d\varphi_\alpha\, dr\right\}$$

But $\int_0^{\pi} L^{(\ell N)}(r,\varphi_\alpha)\,\sin\varphi_\alpha\, d\varphi_\alpha = L^{(\ell N)}(r)$ the spanwise loading

therefore

$$F_x = \mathrm{Re}\left\{N r_o\, e^{i\ell N\Omega t} \int_0^{1} L^{(\ell N)}(r)\,\cos\beta(r)\, dr\right\} \qquad \text{(C-5)}$$

The total force in the y-direction is

$$F_y = \mathrm{Re}\sum_{n=1}^{N} e^{iq(\Omega t-\bar\theta_n)} \int_S\int \Delta P^{(q)}(r,\varphi_o)\sin\beta(r)\,\cos(\Omega t-\varphi_o-\bar\theta_n)\, dS$$

$$= \mathrm{Re}\sum_{n=1}^{N}\frac{1}{2}\int_0^{\pi}\int_r L^{(q)}(r,\varphi_\alpha)\sin\beta(r)\Big[e^{i(q+1)(\Omega t-\bar\theta_n)}e^{i\theta_b^r\cos\varphi_\alpha} + e^{i(q-1)(\Omega t-\bar\theta_n)}e^{-i\theta_b^r\cos\varphi_\alpha}\Big]\cdot\sin\varphi_\alpha\, d\varphi_\alpha\, dr$$

Since $\sum_{n=1}^{N} e^{\pm i(q\pm1)\bar\theta_n} = \begin{cases} N & \text{for } q\pm1 = \ell N \\ 0 & \text{otherwise}\end{cases}$

$$F_y = \mathrm{Re}\left\{\frac{N}{2}e^{i\ell N\Omega t}\int_0^{\pi}\int_r\Big[L^{(\ell N-1)}(r,\varphi_\alpha)e^{i\theta_b^r\cos\varphi_\alpha} + L^{(\ell N+1)}(r,\varphi_\alpha)e^{-i\theta_b^r\cos\varphi_\alpha}\Big]\cdot\sin\beta(r)\,\sin\varphi_\alpha\, d\varphi_\alpha\, dr\right\}$$

The φ_α-integrals are

$$\int_0^{\pi} L^{(\ell N\mp1)}(r,\varphi_\alpha)\, e^{\pm i\theta_b^r\cos\varphi_\alpha}\,\sin\varphi_\alpha\, d\varphi_\alpha$$

$$= \int_0^{\pi}\sum_{\bar n=1} L^{(\ell N\mp1,\bar n)}(r)\,\Theta(\bar n)e^{\pm i\theta_b^r\cos\varphi_\alpha}\sin\varphi_\alpha\, d\varphi_\alpha$$

$$= \sum_{\bar n=1} L^{(\ell N\mp1,\bar n)}(r)\,\Lambda^{(\bar n)}(\mp\theta_b^r) \qquad \text{(C-6)}$$

where $\Lambda^{(\bar n)}(\mp\theta_b^r)$ is given in Appendix A.

Therefore

$$F_y = \mathrm{Re}\left\{ \frac{Nr_o}{2} e^{i\ell N\Omega t} \int_o^1 \sum_{n=1}^{-} \left[L^{(\ell N-1,\bar{n})}(r)\, \Lambda^{(\bar{n})}(-\theta_b^r) + L^{(\ell N+1,\bar{n})}(r)\, \Lambda^{(\bar{n})}(\theta_b^r) \right] \cdot \sin\beta(r)\, dr \right\}$$

The vertical force is

$$F_z = \mathrm{Re}\left\{ \sum_{n=1}^{N} e^{iq(\Omega t-\bar{\theta}_n)} \int_S\int \Delta P^{(q)}(r,\varphi_o)\, \sin\beta(r)\, \sin(\Omega t-\varphi_o-\bar{\theta}_n)\, dS \right\}$$

and following the steps indicated in the development for F_y, the force is finally

$$F_z = \mathrm{Re}\left\{ \frac{-Nr_o}{2i} e^{i\ell N\Omega t} \int_o^1 \sum_{n=1} \left[L^{(\ell N-1,\bar{n})}(r)\, \Lambda^{(\bar{n})}(-\theta_b^r) - L^{(\ell N+1,\bar{n})}(r)\, \Lambda^{(\bar{n})}(\theta_b^r) \right] \cdot \sin\beta(r)\, dr \right\} \qquad \text{(C-8)}$$

The moment about the x-axis (torque) is

$$Q_x = \mathrm{Re}\left\{ - \sum_{n=1}^{N} e^{iq(\Omega t-\bar{\theta}_n)} \int_S\int \Delta P^{(q)}(r,\varphi_o)\, \sin\beta(r)\, r\, dS \right\}$$

and by analogy with F_x this becomes

$$Q_x = \mathrm{Re}\left\{ - Nr_o^2 e^{i\ell N\Omega t} \int_o^1 L^{(\ell N)}(r)\, \sin\beta(r)\, r\, dr \right\} \qquad \text{(C-9)}$$

The bending moment about the y-axis is

$$Q_y = \mathrm{Re}\left\{ \sum_{n=1}^{N} e^{iq(\Omega t-\bar{\theta}_n)} \int_S\int \Delta P^{(q)}(r,\varphi_o) \left[r\varphi_o \tan\beta(r)\, \sin\beta(r)\, \sin(\Omega t-\varphi_o-\bar{\theta}_n) + r\cos\beta(r)\, \cos(\Omega t-\varphi_o-\bar{\theta}_n) \right] dS \right\}$$

which with the trigonometric transformations employed before becomes

$$Q_y = \mathrm{Re}\Bigg\{ \sum_{n=1}^{N} \frac{1}{2} \int_0^{\pi} \int_r^{} L^{(q)}(r,\varphi_\alpha) \Big\{ i\theta_b^r \cos\varphi_\alpha \frac{\sin^2\beta(r)}{\cos\beta(r)} \Big[e^{i(q+1)(\Omega t - \bar{\theta}_n)} e^{i\theta_b^r \cos\varphi_\alpha}$$

$$- e^{i(q-1)(\Omega t - \bar{\theta}_n)} e^{-i\theta_b^r \cos\varphi_\alpha} \Big] + \cos\beta(r) \Big[e^{i(q+1)(\Omega t - \bar{\theta}_n)} e^{i\theta_b^r \cos\varphi_\alpha}$$

$$+ e^{i(q-1)(\Omega t - \bar{\theta}_n)} e^{-i\theta_b^r \cos\varphi_\alpha} \Big] r \sin\varphi_\alpha \, d\varphi_\alpha \, dr \Big\}$$

$$= \mathrm{Re}\Bigg\{ \frac{N}{2} e^{i\ell N\Omega t} \int_r^{} \Big\{ \int_0^{\pi} i\theta_b^r \tan\beta(r) \sin\beta(r) \Big[L^{(\ell N-1)}(r,\varphi_\alpha) e^{i\theta_b^r \cos\varphi_\alpha}$$

$$- L^{(\ell N+1)}(r,\varphi_\alpha) e^{-i\theta_b^r \cos\varphi_\alpha} \Big] \cdot \cos\varphi_\alpha \sin\varphi_\alpha \, d\varphi_\alpha$$

$$+ \int_0^{\pi} \cos\beta(r) \Big[L^{(\ell N-1)}(r,\varphi_\alpha) e^{i\theta_b^r \cos\varphi_\alpha} + L^{(\ell N+1)}(r,\varphi_\alpha) e^{-i\theta_b^r \cos\varphi_\alpha} \Big]$$

$$\sin\varphi_\alpha \, d\varphi_\alpha \Big\} \cdot r \, dr \Bigg\}$$

The first φ_α-integral is

$$\int_0^{\pi} L^{(\ell N \mp 1)}(r,\varphi_\alpha) e^{\pm i\theta_b^r \cos\varphi_\alpha} \cos\varphi_\alpha \sin\varphi_\alpha \, d\varphi_\alpha$$

$$= \int_0^{\pi} \sum_{n=1} L^{(\ell N \mp 1, \bar{n})}(r) \, \Theta(\bar{n}) \, e^{\pm i\theta_b^r \cos\varphi_\alpha} \cos\varphi_\alpha \sin\varphi_\alpha \, d\varphi_\alpha$$

$$= \sum_{n=1} L^{(\ell N \mp 1, \bar{n})}(r) \, \Lambda_1^{(\bar{n})}(\mp\theta_b^r) \qquad \text{(C-10)}$$

where $\Lambda_1^{(n)}(\,)$ is as defined in Appendix A. The second φ_α-integral is given by (C-6). Finally,

$$Q_y = \mathrm{Re}\Big\{ \frac{Nr_o^2}{2} e^{i\ell N\Omega t} \int_0^{1} \Big\{ i\theta_b^r \sin\beta(r) \tan\beta(r) \sum_{n=1} \Big[L^{(\ell N-1,\bar{n})}(r) \, \Lambda_1^{(\bar{n})}(-\theta_b^r)$$

$$- L^{(\ell N+1,\bar{n})}(r) \, \Lambda_1^{(\bar{n})}(\theta_b^r) \Big] + \cos\beta(r) \sum_{n=1} \Big[L^{(\ell N-1,\bar{n})}(r) \Lambda^{(\bar{n})}(-\theta_b^r)$$

$$+ L^{(\ell N+1,\bar{n})}(r) \, \Lambda^{(\bar{n})}(\theta_b^r) \Big] \Big\} \, r \, dr \qquad \text{(C-11)}$$

The bending moment about the z-axis is

$$Q_z = \mathrm{Re}\left\{ \sum_{n=1}^{N} e^{iq(\Omega t-\bar{\theta}_n)} \int\int_{\S} \Delta P^{(q)}(r,\varphi_o)\left[r\varphi_o \tan\beta(r) \sin\beta(r) \cos(\Omega t-\varphi_o-\bar{\theta}_n) \right.\right.$$

$$\left.\left. - r \cos\beta(r) \sin(\Omega t-\varphi_o-\bar{\theta}_n)\right] dS \right\}$$

It can be shown that

$$Q_z = \mathrm{Re}\left\{\frac{-Nr_o^2}{2i} e^{i\ell N\Omega t} \int_o^1 \left\{ i\theta_b^r \sin\beta(r) \tan\beta(r) \sum_{\bar{n}=1} \left[L^{(\ell N-1,\bar{n})}(r) \Lambda_1^{(\bar{n})}(-\theta_b^r) \right.\right.\right.$$

$$\left. + L^{(\ell N+1,\bar{n})}(r) \Lambda_1^{(\bar{n})}(\theta_b^r)\right] + \cos\beta(r) \sum_{n=1} \left[L^{(\ell N-1,\bar{n})}(r) \Lambda^{(\bar{n})}(-\theta_b^r) \right.$$

$$\left.\left.\left. - L^{(\ell N+1,\bar{n})}(r) \Lambda^{(\bar{n})}(\theta_b^r)\right]\right\} \cdot r\, dr\right\} \qquad \text{(C-12)}$$

In the text, and in the program as well, the hydrodynamic pitch angle $\beta(r)$ of the assumed helicoidal surface is replaced by the geometric pitch angle $\theta_p(r)$ of the actual propeller.

APPENDIX D

THE SINGULARITIES OF THE INTEGRANDS OF THE BLADE PRESSURE DISTRIBUTION

In Equation (49) for the pressure due to thickness (non-lifting) it is seen that there is a singularity when $\rho = r$, $x = \xi$, $\theta_o = \varphi_o$ and $\bar{\theta}_n = 0$ (i.e., $n = 1$). The singular part of the pressure can be expressed as (see Eq. (53) with the substitutions $\theta_o = a\xi$ and $\varphi_o = ax$):

$$P_{T_1} = i \frac{\rho_f U^2}{2\pi^2} \int_0^{\pi} \int_{\rho} \frac{\partial f(\rho,\theta_\alpha)}{\partial \theta_\alpha} \sqrt{1+a^2\rho^2} \left\{ \int_{-\infty}^{\infty} k(IK)_o e^{ik(x-\xi)} dk \right.$$

$$\left. + \sum_{m=1}^{\infty} \int_{-\infty}^{\infty} (IK)_m \left[(k-am) e^{i(k-am)(x-\xi)} + (k+am) e^{i(k+am)(x-\xi)} \right] dk \right\} d\theta_\alpha d\rho \tag{D-1}$$

For arbitrary thickness (see Eq. (32)).

$$\frac{\partial f(\rho,\theta_\alpha)}{\partial \theta_\alpha} \approx C_o(\rho) \cos \frac{\theta_\alpha}{2} + \sum_{n=1}^{4} C_n(\rho) \sin n\theta_\alpha$$

where the coefficients are obtained as shown in sect. A,3,c. Then the trigonometric transformation

$$\xi = (\sigma^\rho - \theta_b^\rho \cos\theta_\alpha)/a$$

yields

$$\cos\theta_\alpha = \frac{\sigma^\rho - a\xi}{\theta_b^\rho}$$

$$\cos \frac{\theta_\alpha}{2} = \sqrt{\frac{\theta_b^\rho + \sigma^\rho - a\xi}{2\theta_b^\rho}}$$

$$\sin\theta_\alpha \, d\theta_\alpha = \frac{a}{\theta_b^\rho} d\xi$$

$$\sin 2\theta_2 \, d\theta_\alpha = 2\sin\theta_\alpha \cos\theta_\alpha \, d\theta_\alpha = \frac{2a(\sigma^\rho - a\xi)d\xi}{(\theta_b^\rho)^2}$$

$$\sin 3\theta_\alpha d\theta_\alpha = \left[-1+4\frac{(\sigma^\rho - a\xi)^2}{(\theta_b^\rho)^2}\right] \frac{a}{\theta_b^\rho} \, d\xi$$

$$\sin 4\theta_\alpha = \left[8\left(\frac{\sigma^\rho - a\xi}{\theta_b^\rho}\right)^3 - 4\left(\frac{\sigma^\rho - a\xi}{\theta_b^\rho}\right)\right] \frac{a}{\theta_b^\rho} \, d\xi$$

and thus the slope can be expressed in the following form:

$$\frac{\partial f}{\partial \theta_\alpha}(\rho, \theta_\alpha) d\theta_\alpha \simeq \left\{\left[d_o(\rho) + \sqrt{d_1(\rho) - d_2(\rho)\xi} + d_3(\rho)\xi + d_4(\rho)\xi^2 + d_5(\rho)\xi^3\right] d\xi\right.$$

$$= \frac{F(\xi,\rho)}{\sqrt{1+a^2\rho^2}} \, d\xi$$

Equation (D-1) can be written as

$$P_{\tau_1} = \frac{i\rho_f U^2}{2\pi^2} \int_\xi \int_\rho F(\xi,\rho) \left\{ \int_{-\infty}^{\infty} k(IK)_o \, e^{ik(x-\xi)} dk \right.$$

$$\left. + \sum_{m=1}^{\infty} \int_{-\infty}^{\infty} (IK)_m \left[(k-am)e^{i(k-am)(x-\xi)} + (k+am)e^{i(k+am)(x-\xi)}\right] dk \right\} \, d\xi d\rho$$

(D-2)

For finite m the expansion of $1/R$ in the above has no singularity. The singular behavior is present only in the infinite m-series (see Reference 10). When $m \geq M$ large, the generalized mean value theorem can be used:

$$\int_c^d f(k)\, p(k)\, dk \approx f(A) \int_c^d p(k)\, dk, \quad c \leq A \leq d$$

where $f(k) = \begin{cases} I_m(|k|\rho)\, K_m(|k|r) & \text{for } \rho < r \\ I_m(|k|r)\, K_m(|k|\rho) & \text{for } r < \rho \end{cases}$

and $f(A) = I_m(|A|\rho)\, K_m(|A|r)$, etc. with $A << m$ (order).

By using Nicholson's[11] approximation for the product of the modified Bessel functions when $A << m$

$$f(A) \approx \frac{1}{2m} Z^m \text{ where } Z = \begin{cases} \rho/r & \text{for } \rho < r \\ r/\rho & \text{for } r < \rho \end{cases} \qquad \text{(D-3)}$$

Then for large m the integral can be written as

$$I = \int_\xi \int_\rho F(\xi,\rho) \sum_{m=M}^{\infty} \frac{1}{m} Z^m \left\{ \cos am(x-\xi) \int_{-\infty}^{\infty} k e^{ik(x-\xi)} dk \right.$$

$$\left. + i\, a\, m \sin am(x-\xi) \int_{-\infty}^{\infty} e^{ik(x-\xi)} dk \right\} d\xi\, d\rho \qquad \text{(D-4)}$$

From Jolley's collection of series summations[12]

$$ia \sum_{m=1}^{\infty} Z^m \sin ma(x-\xi) = \frac{iaZ \sin a(x-\xi)}{1-2Z\cos a(x-\xi)+Z^2} \quad \text{(see Jolley 499)}$$

Also $$\frac{\partial}{\partial Z} \sum_{m=1}^{\infty} \frac{1}{m} Z^m \cos ma(x-\xi) = \frac{1}{Z} \sum_{m=1}^{\infty} Z^m \cos ma(x-\xi)$$

$$= \frac{\cos a(x-\xi) - Z}{1-2Z\cos a(x-\xi)+Z^2} \quad \text{(see Jolley 500)}$$

Therefore

$$\sum_{m=1}^{\infty} \frac{1}{m} Z^m \cos ma(x-\xi) = \int \frac{\cos a(x-\xi) - Z}{1-2Z\cos a(x-\xi)+Z^2}\, dz$$

$$= -\frac{1}{2} \log \left[1 - 2Z\cos a(x-\xi)+Z^2\right]$$

The m-series of (D-4) then is equivalent to

$$S_m = \left\{ -\frac{1}{2} \log \left[1-2z\cos a(x-\xi)+Z^2\right] \int_{-\infty}^{\infty} k e^{ik(x-\xi)} dk \right.$$

$$\left. + \frac{iaZ\sin a(x-\xi)}{1-2\,Z\cos a(x-\xi)+Z^2} \int_{-\infty}^{\infty} e^{ik(x-\xi)}\, dk \right\}$$

$$- \sum_{m=1}^{M} \frac{1}{m} Z^m \left\{ \cos am(x-\xi) \int_{-\infty}^{\infty} k\, e^{ik(x-\xi)}\, dk \right.$$

$$\left. + i\, am \sin am(x-\xi) \int_{-\infty}^{\infty} e^{ik(x-\xi)dk} \right\} \qquad \text{(D-5)}$$

where the finite m-series can be ignored since it is certainly not singular.

The k-integrals are evaluated as

$$\int_{-\infty}^{\infty} e^{ik(x-\xi)} dk = 2\pi\, \delta(x-\xi)$$

$$\int_{-\infty}^{\infty} k\, e^{ik(x-\xi)}\, dk = -\, i2\pi\, \delta'(x-\xi) \qquad \text{(D-6)}$$

where $\delta(x-\xi)$ is the Dirac delta function and $\delta'(x-\xi)$ the derivative of this function with respect to $(x-\xi)$.

With the substitution of (D-5) and (D-6) and letting $x_o = x - \xi$, Equation (D-4) becomes

$$I = i2\pi \int_{x_o} \int_{\rho} F(x-x_o,\rho) \left\{ -\frac{1}{2} \log\left(1-2Z\cos ax_o+Z^2\right) \delta'(x_o) \right.$$

$$\left. - \frac{aZ \sin ax_o}{1-2Z\cos ax_o+Z^2}\, \delta(x_o) \right\} dx_o\, d_\rho \qquad \text{(D-7)}$$

and integrating over x_o results in

$$I = +i\pi \int_{\rho} \frac{\partial F(x-x_o)\rho)}{\partial x_o}\bigg|_{x_o=o} \log\left(1-2Z+Z^2\right) d\rho \qquad \text{(D-8)}$$

With $z = \rho/r$ or r/ρ,

$$\log(1-2Z+Z^2) = \log(1-Z)^2 = 2\log(1-Z)$$

$$= 2\log\left(\frac{r-\rho}{r}\right) \text{ or } 2\log\left(\frac{\rho-r}{\rho}\right)$$

hence the ρ-integral has a logarithmic singularity when $\rho \to r$ and this has a finite contribution and is integrable.

APPENDIX E

EVALUATION OF THE ρ-INTEGRATION IN THE REGION OF THE SINGULARITY (SECTION B)

Let $\bar{K}(\rho)$ represent the integrand of the ρ-integration. It has been seen that when $\rho \to r$, $\bar{K}(\rho)$ varies as $\ell n(\rho-r)$. A logarithmic singularity is integrable, but since the integration is performed numerically, special precautions must be taken. In the region of the singularity $\rho = r$, the integral is put in the form

$$I = \int_{r-\beta}^{r+\beta} \frac{M(\rho)}{\rho-r}\, d\rho \qquad \text{(E-1)}$$

where $M(\rho) = (\rho-r)\bar{K}(\rho)$ so that $M = 0$ when $\rho = r$, and $\beta = \Delta r/2$.

The function $M(\rho)$ can be expanded about the singularity $\rho = r$ by the Lagrange formula

$$M(\rho) = \sum_{i=o}^{n} \frac{\Pi_n(\rho)}{(\rho-\rho_i)\ \Pi_n'(\rho_i)}\ M_{i+1} \quad i = 0,\ 1,\ldots.n \qquad \text{(E-2)}$$

where

$$\Pi_n(\rho) = (\rho-\rho_o)\ (\rho-\rho_1)\cdots\cdot(\rho-\rho_n)$$

$$\Pi_n'(\rho_i) = \frac{d}{d\rho}\,\Pi_n(\rho) \quad \text{evaluated at } \rho = \rho_i$$

and $M_{i+1} = M(\rho_i)$ (see Scarborough[13] and Watkins et al[14]).

In the strip from $r - \beta$ to $r + \beta$ (with $n = 4$ for the 5-point formula), $\rho_o = r - \beta = r - 2\delta$, $\rho_1 = r - \delta$, etc. where $\delta = \beta/2$. Then

$$\Pi_n'(\rho_i) = (-1)^{4-i}\ \delta^4\ i!\ (4-i)! \qquad \text{(E-3)}$$

and

$$M(\rho) = \frac{1}{\delta^4} \sum_{i=o}^{4} \frac{(-1)^i}{i!\,(4-1)!} \frac{(\rho-r+2\delta)\,(\rho-r+\delta)\,(\rho-r)\,(\rho-r-\delta)\,(\rho-r-2\delta)}{\rho - r + (2-i)\delta}\ M_{i+1}$$

(E-4)

where $M_3 = 0$ since $\rho_2 = r$.

The integral is

$$I = \int_{r-2\delta}^{r+2\delta} \frac{M(\rho)}{(\rho-r)}\, d\rho = \frac{1}{\delta^4} \int_{r-2\delta}^{r+2\delta} [g_o(\rho-r)^3+\delta g_1(\rho-r)^2+\delta^2 g_2(\rho-r)+\delta^3 g_3+ \frac{\delta^4 g_4}{\rho-r}]d\rho \qquad \text{(E-5)}$$

where

$$g_o = \frac{M_1 + M_5}{4!} - \frac{M_2 + M_4}{3!} + \frac{M_3}{2!}$$

$$g_1 = \frac{2(M_5 - M_1)}{4!} - \frac{(M_4 - M_2)}{3!}$$

$$g_2 = \frac{-(M_1 + M_5)}{4!} + \frac{4(M_2 + M_4)}{3!} - \frac{5M_3}{2!2!} \qquad \text{(E-6)}$$

$$g_3 = \frac{2(M_1 - M_5)}{4!} - \frac{4(M_2 - M_4)}{3!}$$

$$g_4 = \frac{4}{2!2!}\, M_3 \quad (M_3 = 0)$$

then $$I = \frac{1}{\delta^4}\left\{\frac{\delta g_1}{3}\, 2(2\delta)^3 + \delta^3 g_3\, 2(2\delta)\right.$$

$$= \frac{16}{3}\, g_1 + 4g_3$$

or $$I = \frac{1}{9}\,(M_5-M_1) + \frac{16}{9}\,(M_4-M_2) \qquad \text{(E-7)}$$

where $M_1 = -\beta\, \bar{K}_1 (\rho = r - \beta)$

$M_2 = -\frac{\beta}{2}\, \bar{K}_2 \quad (\rho = r - \frac{\beta}{2})$

$M_4 = +\frac{\beta}{2}\, \bar{K}_4 \quad (\rho = r + \frac{\beta}{2})$

$M_5 = +\beta\, \bar{K}_5 \quad (\rho = r + \beta)$

Therefore

$$1 = \frac{1}{9}\frac{\Delta r}{2}\left(\bar{K}_5+\bar{K}_1\right) + \frac{16}{9}\frac{\Delta r}{4}\left(\bar{K}_4+\bar{K}_2\right)$$

and

$$\frac{1}{\Delta r} = \frac{1}{18}\left(\bar{K}_5+\bar{K}_1\right) + \frac{4}{9}\left(\bar{K}_4+\bar{K}_2\right) \qquad \text{(E-8)}$$